HHS Public Access

Author manuscript

Free Radic Biol Med. Author manuscript; available in PMC 2020 September 01.

Published in final edited form as:

Free Radic Biol Med. 2019 September ; 141: 115–140. doi:10.1016/j.freeradbiomed.2019.05.033.

Human myeloperoxidase (hMPO) is expressed in neurons in the substantia nigra in Parkinson's disease and in the hMPO-α-synuclein-A53T mouse model, correlating with increased nitration and aggregation of α-synuclein and exacerbation of motor impairment.

Richard A Maki[1], **Michael Holzer**[2], **Khatereh Motamedchaboki**[3], **Ernst Malle**[4], **Eliezer Masliah**[5,6,7], **Gunther Marsche**[2], **Wanda F. Reynolds**[1]

[1]Sanford Burnham Prebys Medical Discovery Institute, La Jolla, California, USA

[2]Otto Loewi Research Center, Division of Pharmacology, Medical University of Graz, Austria

[3]Tumor Initiation & Maintenance Program and NCI Cancer Centre Proteomics Facility, Sanford Burnham Prebys Medical Discovery Institute, La Jolla, CA, USA

[4]Gottfried Schatz Research Center, Division of Molecular Biology and Biochemistry, Medical University of Graz, Austria

[5]Molecular Neuropathology Section, Laboratory of Neurogenetics, National Institute on Aging, National Institutes of Health, Bethesda, MD, 20892, USA.

[6]Department Neurosciences, School of Medicine, University of California, San Diego, La Jolla, CA, 92093, USA.

[7]Department of Pathology, School of Medicine, University of California, San Diego, La Jolla, CA, 92093, USA.

Abstract

α-Synuclein (αSyn) is central to the neuropathology of Parkinson's disease (PD) due to its propensity for misfolding and aggregation into neurotoxic oligomers. Nitration/oxidation of αSyn leads to dityrosine crosslinking and aggregation. Myeloperoxidase (MPO) is an oxidant-generating enzyme implicated in neurodegenerative diseases. In the present work we have examined the impact of MPO in PD through analysis of postmortem PD brain and in a novel animal model in which we crossed a transgenic mouse expressing the human MPO (hMPO) gene to a mouse expressing human αSyn -A53T mutant (A53T) (hMPO-A53T). Surprisingly, our results show that in PD substantia nigra, the hMPO gene is expressed in neurons containing aggregates of nitrated αSyn as well as MPO-specific HOCl-modified epitopes. In our hMPO-A53T mouse model, we also saw hMPO expression in neurons but not mouse MPO. In the mouse model, hMPO was

Corresponding Author: 858-795-5127; wreynolds@sbpdiscovery.org.

expressed in neurons colocalizing with nitrated αSyn, carbamylated lysine, nitrotyrosine, as well as HOCl-modified epitopes/proteins. RNAscope in situ hybridization confirmed hMPO mRNA expression in neurons. Interestingly, the hMPO protein expressed in hMPO-A53T brain is primarily the precursor proMPO, which enters the secretory pathway potentially resulting in interneuronal transmission of MPO and oxidative species. Importantly, the hMPO-A53T mouse model, when compared to the A53T model, exhibited significant exacerbation of motor impairment on rotating rods, balance beams, and wire hang tests. Further, hMPO expression in the A53T model resulted in earlier onset of end stage paralysis. Interestingly, there was a high concentration of αSyn aggregates in the stratum lacunosum moleculare of hippocampal CA2 region, which has been associated in humans with accumulation of αSyn pathology and neural atrophy in dementia with Lewy bodies. This accumulation of αSyn aggregates in CA2 was associated with markers of endoplasmic reticulum (ER) stress and the unfolded protein response with expression of activating transcription factor 4 (ATF4), C/EBP homologous protein (CHOP), MPO, and cleaved caspase-3. Together these findings suggest that MPO plays an important role in nitrative and oxidative damage that contributes to αSyn pathology in synucleinopathies.

Graphical Abstract

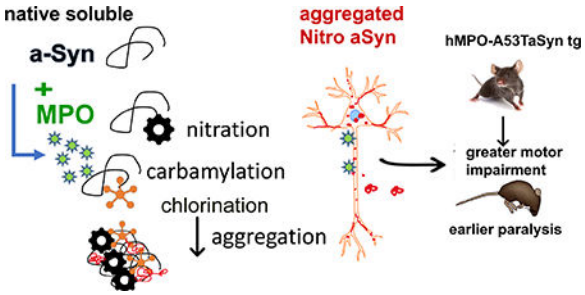

Keywords

Myeloperoxidase; Reactive oxygen species; Synucleinopathies; Nitration; Carbamylation; Hypochlorous acid; MPO-H2O2-chloride system; Parkinson's disease; Alpha synuclein; Hippocampus CA2 region; Dementia with Lewy Bodies; ER stress; Unfolded protein response

1. Introduction

Parkinson's disease (PD), the second most common neurodegenerative disease, is associated with the selective loss of dopaminergic neurons in the substantia nigra (SN) pars compacta (SNpc) leading to tremor, bradykinesia, rigidity, and postural instability (reviewed [1, 2]). Like other major neurodegenerative diseases, PD is considered a protein misfolding disorder. Compelling evidence, both histopathological and epidemiological, implicate α-synuclein (αSyn) oligomers and aggregates as the primary cause of PD. The histological hallmark of PD are Lewy bodies, proteinaceous inclusions comprised primarily of aggregated nitrated αSyn [3]. Single point mutations (such as A53T) or duplications of the αSyn gene are linked to rare familial forms of PD, indicating increased levels of αSyn are sufficient to cause the disease (reviewed [4, 5]). αSyn is normally a soluble protein with native unfolded conformation yet is prone to self-aggregation into neurotoxic oligomers and fibrils [6]. The

mechanisms leading to αSyn aggregation are not fully understood but evidence points to oxidative stress [7–11]. The SNpc in PD has been associated with increased levels of lipid peroxidation and 4-hydroxynonenal [9], as well as 3-nitrotyrosine [10], malondialdehyde [12], protein carbonyls [13], and the oxidized nucleic acid product 8-hydroxyguanosine [14]. Nitration/oxidation of αSyn is known to promote its misfolding and aggregation [15, 16]. αSyn is primarily localized to the presynaptic terminus of neural axons, where oxidation and dimerization could impair its potential role in synaptic function and neurotransmitter release [17–19]. Sources for reactive oxygen species in PD include mitochondrial complex I dysfunction, iron, reactive astrocytes, and microglia [20].

Myeloperoxidase (MPO) also generates reactive oxygen and nitrogen species [21], and increased levels of MPO have been found in PD brain [22]. MPO is a component of the armamentarium of the innate immune system, present at high levels in storage vesicles in phagocytes. When neutrophils and monocytes engulf microbes, the MPO-containing vesicles fuse with the phagosome releasing the enzyme which reacts in the presence of hydrogen peroxide (H_2O_2) with chloride ions (Cl^-) to produce the potent oxidant, hypochlorous acid (HOCl)(bleach) [23, 24].

While MPO generated oxidants are microbicidal and thus beneficial, these oxidants can also damage normal cells. MPO is generally considered a myeloid specific gene with expression restricted to bone marrow myeloid precursors, but the human MPO (hMPO) gene can escape this restriction in some stress situations, such as in microglia, astrocytes and neurons in Alzheimer's Disease (AD) [25–27] and in astrocytes in PD [22, 28]. In order to study the effects of hMPO expression in mouse models of neurodegenerative diseases, we created a humanized mouse model transgenic for a single copy of the hMPO gene in a 32 kb restriction fragment [29]. When this mouse strain was crossed to an amyloid precursor protein (APP) overexpressing model of AD (APP23), the hMPO transgene was expressed robustly in astrocytes [26]. This atypical expression of hMPO is thought to be due in part to the insertion in the promoter of an Alu element encoding several overlapping binding sites for members of the nuclear receptor superfamily of transcription factors as well as SP1 [30–33]. A polymorphism in these Alu nuclear receptor sites, −463G, increases hMPO expression and has been linked to the risk for AD [25, 34–38], cardiovascular disease [39–44], lung cancer [45, 46], and some epithelial cancers [47]. The murine MPO (mMPO) gene, lacking the primate-specific Alu, is expressed at relatively low levels in mouse models of AD [26] and, as shown here, in an A53T-αSyn overexpressing model of PD.

In this study we set out to investigate the involvement of MPO in PD through analysis of human PD brain tissue and the hMPO-A53T mouse model. The results provide the first evidence that MPO expression occurs in neurons in PD SNpc as well as in the hMPO-A53T model. In the hMPO-A53T model, MPO promotes αSyn nitration and carbamylation, associated with increased aggregation of αSyn and greater motor impairment, correlating with earlier onset of paralysis and death.

2. Materials and Methods

2.1 Reagents

Reagents included NuPage 4–12% Bis-Tris gels (NP0322), MOPS-SDS running buffer (NP0001), NuPAGE LDS sample buffer (NP0008), and DAPI (4', 6-diamidino-2-phenylindole) (D-1306), TaqMan gene expression master mix and Taqman primer/probes (Applied Biosystems) including mouse glyceraldehyde-3-phosphate dehydrogenase (GAPDH), (4326317E), mouse beta 2 microglobulin (Mm00437762_m1), mMPO, (Mm00447886_m1), hMPO (Hs00165162_m1), murine αSyn (mαSyn, Mm01188700_m1), and human αSyn (hαSyn, Hs00240906_m1). For cell culture, we used Neurobasal Plus medium, B27 supplement, and penicillin/streptomycin from Life Technologies. hαSyn protein (AG938) was from EMD Millipore North America. hMPO (426–10) was from Lee Biosolutions. Lightning-Link HRP antibody labeling kit (701–0030) was from Novus Biologicals. The probe for hMPO (469561) for *in situ* hybridization was from Advanced Cell Diagnostics. The MPO ELISA kit was from ALPCO. Dynabeads magnetic sheep anti-rabbit Protein A/G beads were from Invitrogen (112.03D), and BCA protein reagent (23227) was from Pierce. Protran™ nitrocellulose (10600007), cellulose acetate (OE66), and Sepharose 4B (17043002) was from GE-Healthcare. Non-fat dry milk (Blotto; B5001) was from Rockland, Inc. Complete™ protease inhibitor cocktail tablets with and without EDTA (04693124001, 04693159001) were from Roche. The surfactants Tween-20 (P7949), NP40 (NP40S) and Triton X-100 (T8787), serine protease inhibitor PMSF (P7626), potassium cyanate, deoxyribonuclease I (D5025) and sodium nitrite were from Sigma. The ECL reagent, WesternBright™ Sirius Western Blotting horseradish peroxidase (HRP) substrate (K12043), was from Advansta. Blue Devil™ autoradiography film (30–101) was from Genesee Scientific. Vectashield™ mounting media (H-1000) was from Vector Labs. Non-immune donkey or horse serum (017-000-121, 008-000-121) were obtained from Jackson Immunoresearch Labs. Bovine serum albumin (BSA) (BP1600100) for Western blots, Halt protease inhibitors, and Syn-Per (87793) as well as all general chemicals used for these studies were from Thermo Fisher.

2.2 Transgenic mice

Transgenic mice carrying the human −463G MPO allele have been previously described [29, 30, 32, 48]. There is one copy of the hMPO −463G allele in the mouse genome on the X chromosome. The mice were generated by microinjection of a 32 kb BST11071 restriction fragment into C57BL6/J eggs [29]. Mice overexpressing the human A53T αSyn mutant gene under control of the human thymus cell antigen 1 (Thy1) promoter (THY1-SNCA*A53T)M53SUD/J) (Jackson, 008135) have been described [49–51]. Mice overexpressing the wild-type hαSyn gene driven by the mouse Thy1 promoter (mThy1-α-syn, Line 61) and the mice overexpressing hαSyn driven by the platelet derived growth factor (PDGF) promoter have been described [52–54]. Mice overexpressing the hαSyn mutant gene under control of the mouse myelin basic protein promoter (MBP) have also been described in a model of multiple systems atrophy (MSA) [55]. The primers for genotyping the mice are: hMPO for: 5'-GCAATGGTTCAAGCGATTCTT-3'; hMPO rev: 5'-CGGTATAGGCACACAATGGTGAG-3'; hSNCA for: 5'-

GGCACCTAGAGGATCTCGACTAGTGG-3'; Thy1-SNCA rev: 5'-GATGATGGCATGCAGCACTGG-3'.

2.3 Antibodies

Primary antibodies used in this study included rabbit anti-hMPO (DAKO A0398, 1/500 for immunohistochemistry (IHC) and 1/1000 for Western blots (WB)), goat anti-hMPO that is affinity purified against hMPO (R&D Systems, AF3174, 1/500 IHC and 1/2000 WB). These antibodies have been used in a number of studies involving MPO including a recent report in which we showed the DAKO rabbit and R&D goat MPO antibodies recognize MPO in immunoblots or immunostains of T47D cells transfected with hMPO expression construct but did not recognize nontranfected T47D cells [56].

Other antibodies used in this study include Mab αSyn D37A6 (Cell Signaling, D37A6, 1/500 IHC and 1/2000 WB), Mab αSyn (BD Biosciences, 6107877; 1/500 IHC and 1/2000 WB), Mab anti-nitrated αSyn (Syn505, Life Technologies, 358300, 1/500 IHC and 1/2000 WB), [57], Mab anti-αSyn raised against Lewy bodies which recognizes an epitope encoded by amino acids 115–122, and recognizes human but not mouse αSyn (LB509, Santa Cruz, sc-58480, 1/100 IHC and 1/1000 WB) [58], rabbit anti-nitrotyrosine (nitroTyr, Millipore, AB5411, 1/200 IHC and 1/1000 WB), Mab anti-nitro-α/β-synuclein (Tyr^{39}) clone nSyn14 (Millipore-Sigma, 36–012 1/200 IHC) [59], rabbit monoclonal antibody NeuN (Cell Signalling D4G40, 1/200 IHC), rabbit anti-MAP2 (Cell Signalling, 4542, 1/200 IHC), Mab raised against HOCl-modified proteins (clone 2D10G9) [60, 61] (1/50 IHC), rabbit anti-activating transcription factor 4 (ATF4, Cell Signaling, 11815, 1/100 IHC), anti-C/EBP homologous protein (CHOP, Santa Cruz, sc-7351, 1/100 IHC), and anti-cleaved caspase 3 (Cell Signaling, D175, 1/100 IHC). Secondary antibodies labeled with Alexa Fluor 488 (donkey anti-rabbit, A21206 and donkey anti-mouse, A21202) and Alexa Fluor 594 (donkey anti-rabbit, 21207 and donkey anti-mouse, A21203) were from Molecular Probes, goat or donkey anti-mouse HRP and anti-rabbit HRP-conjugated IgG were from Jackson ImmunoResearch. The monoclonal antibody against HOCl-modified epitopes (clone 2D10G9) has been previously validated [60, 62].

2.4 Immunohistochemistry (IHC) and MPO ELISA

Mice were sacrificed by exposure to CO_2, then transcardially perfused with ice cold phosphate buffered saline (PBS). Mouse brain tissue was fixed overnight in 4% paraformaldehyde (PFA) in PBS. Free floating (40 microns) sagittal or coronal sections, obtained with a Leica VT1000S vibrating microtome, were incubated with 10% H_2O_2 in PBS for 10 min, blocked with 10% non-immune goat serum for 12 h, and incubated overnight at 4°C with primary antibodies in the presence of non-immune serum from the secondary antibody host [54, 63]. Primary antibodies were detected with biotinylated secondary antibodies and avidin-conjugated horseradish peroxidase (Vectastain ABC kit, Vector Laboratories, Burlingame, CA) and detected with peroxidase chromogen (SG or DABN) or 3-amino-9-ethylcarbazole, Vector Laboratories).

Paraffin-embedded sections of human (see below) or mouse brains were cleared by xylene and ethanol prior to heat induced antigen retrieval in 10 mM sodium citrate buffer, 0.05 %

Tween 20, pH 6.0. Sections were incubated in 10 % normal donkey serum for 1 h, followed by incubation for 12 h in primary antibodies in PBST and 10 % non-immune donkey serum. Following incubation, the sections were washed in PBST for 2 h prior to incubation with secondary fluorescent donkey antibodies conjugated to Alexa Fluor 488 (green) or Alexa Fluor 594 (red) at 1:3,000 dilution for 1 h. Images were obtained on a conventional fluorescent microscope (Olympus BX51 with 20x, 40x, and 100x objectives) as well as a Zeiss LSM 710 Confocal Microscope using 40x or 63x oil objectives. Images were saved as tiff files in 8-bit per channel format (24-bit RGB) and processed with PhotoshopTM for assembly of figures.

Nonfluorescent immunostaining of paraffin sections was carried out with primary antibodies in PBS + 0.05% Tween 20 (PBST) with 10 % non-immune donkey serum, followed by biotinylated secondary donkey antibodies (Vector) (1:200, 1 h) and avidin-biotin conjugates (Vector Elite ABC system) (1:200, 2 h), and developed with peroxidase substrate as detailed above. All sections were processed simultaneously under the same conditions and each experiment was repeated at least three times with multiple biological replicates. All images present in this manuscript are representative of at least three independent immunostaining experiments.

To quantify the level of MPO in the brains of the mice we performed an MPO ELISA. For the ELISA experiments mice were sacrificed, perfused with ice cold PBS and the brains removed. The brains were homogenized in Tris-NaCl buffer (50 mM Tris-HCl, pH 7.5, 150 mM NaCl, 1% Triton) containing ThermoFisher Halt protease inhibitors and PMSF (1 mM). Samples were centrifuged at 10,000 rpm for 20 min. The supernatant was stored at −80 C until used for the ELISA. The manufacturer’s instructions were followed to determine the levels of MPO in the extracts (ALPCO). The assays were run in duplicate. Protein concentrations were determined by the BCA reaction. Data collected were analyzed using Graph Pad Prizm software.

2.5 Human brain tissue

Autopsy material was obtained from donor patients at the UCSD Neurosciences Department/University of California, San Diego (San Diego, CA) and from the Harvard Brain Tissue Resource Center (Belmont, MA). Aged normal control and mild to late stage PD SN were processed and evaluated according to standard methods [64]. Human tissue was provided without personal identifiers.

2.6 Quantitative Immunohistochemical analysis

Immunostained sections were analyzed with a digital Olympus bright-field and fluorescence microscope (BX51). For each analysis, a minimum of five mice of each genotype was used. For each mouse, a minimum of three paraffin sections was analyzed. In each section, four areas in cortex or other regions were imaged. Quantitation of immunoreactivity was determined by optical density analysis using ImageJ/FIJI software. Levels of optical density were corrected to background using sections that lacked exposure to the primary antibody. After correction to background, the levels of immunoreactivity were expressed as corrected optical density relative units. Statistical analysis was conducted using GraphPad Prism and

Student's t-test for comparing the means of two samples or one-way ANOVA with posthoc Dunnet when comparing the MPO-A53T and A53T tg mice versus wildtype.

Counting of immunostained neurons in sections of mouse hippocampus or cortex was carried out by investigators blinded to genotype and was performed with five mice from each genotype, a minimum of three sections from each brain, and four images per section. Quantitation of immunopositive neurons in human brain sections was performed with paraffin sections of PD SN from eight PD and eight aged control brains. Percent of immunopositive cells was determined from a minimum of three sections from each donor, spaced by 12 sections, and four digital images were analyzed from each section. Counting of immunopositive neurons was performed by investigators blinded to PD status.

2.7 Animals

All animal work was carried out at the AAALAC accredited animal facility at the Sanford-Burnham-Prebys Medical Discovery Institute. The care of the mice, and all the procedures performed were approved by the Institutional Animal Care and Use Committee (protocol number 15–097), and complied with National Institutes of Health animal care guidelines. Animals were housed in individually ventilated cages on standard bedding under a constant 12 h light/dark cycle. Temperature was maintained at 21 °C. Each mouse was examined regularly for signs of distress. All experiments were performed with mice hemizygous for the hMPO or αSyn transgenes. Male mice were used for all of these studies due to the fact that the hMPO transgene is on the X chromosome resulting in random inactivation of one MPO allele on an X chromosome in female mice. Behavior tests used mice ranging in age from 45 to 60 days. Data collected were analyzed using Graph Pad Prizm software.

The hMPO transgenic model was originally created by microinjection into C57Bl6/J eggs. These were crossed to A53T and backcrossed more than ten generations onto C57Bl6/J strain. Mice are maintained as heterozygotes so that litters produce wildtype controls along with hMPO and A53T mice. Wildtype and hMPO A53T littermates are compared in behavior assays, IHC, or other experiments.

2.8 Wire hanging test

The mouse was placed on the top of a standard cage lid that was then shaken gently to induce the mouse to grip the wires, and then inverted for up to 60 s. The lid was elevated 3 ft over soft bedding. Three consecutive trials were performed with a 5 min resting period between each trial. The latency to fall from the cage lid was recorded. Behavior data were analyzed using a one-way analysis of variance (ANOVA) followed by Dunnets post-hoc test using GraphPad Prism v8.

2.9 RotaRod

The test assesses motor coordination of mice placed on a five lane rotating rod (San Diego Instruments) that accelerates slowly from 2 to 20 rpm over a period of 300 s. The instrument records the latency to fall and the rotator speed at fall. The mice were trained on the device for 5 min at a constant speed of 5 rpm for 3 days prior to the experiment. In the experiment, the mice were placed on the RotaRod for up to 300 sec for three consecutive trials with a 5

min rest between trials. Behavior data were analyzed using a one-way analysis of variance (ANOVA) followed by Dunnets post-hoc test using GraphPad Prism v8.

2.10 Balance beam

Mice were trained to walk across an elevated round beam of 1 m length and 1 cm diameter. The beam was elevated 3 ft above the bench with soft padding placed below. Animals were trained three times on the beam one day before the test. All mice were given three consecutive trials. If a mouse paused on the beam it was gently touched on the hindquarters to encourage movement. If the animal fell off the beam the timer was paused and the animal was placed back on the beam at the position it had when it fell. Between each mouse trial, the beam was cleaned with water. Behavior data were analyzed using a one-way analysis of variance (ANOVA) followed by Dunnets post-hoc test using GraphPad Prism v8.

2.11 Survival analysis

hMPO-A53T and A53T mice were observed on a daily basis for the onset of symptoms including partial paralysis of hind quarters and reduced ambulation. The end point was the onset of limb paralysis. For survival curve statistical analysis we used log-rank (Mantel-Cox) test with Graph Pad Prism software.

2.12 Immunoprecipitation assay

Immunoprecipitation studies of MPO from brain regions including cortex/hippocampus, midbrain/thalamus/striatum, or cerebellum/brainstem were performed. The brain tissues were dounce homogenized in five volumes of lysis buffer (50 mM Tris-base, 150 mM NaCl, 1% Triton X-100) with protease inhibitors (Roche) and clarified by centrifugation at 15,000 × g for 20 min. Protein concentration was determined by BCA reagent and equal amounts of total protein were used in the immunoprecipitation. Rabbit polyclonal anti-human MPO antibodies (Dako) were added (2 μg) μl) to the extract overnight at 4°C, and then pulled down with sheep anti-rabbit IgG coupled to protein A/G magnetic beads (Dynabeads) for 2 h. The beads were washed twice for 20 min in PBS + 0.01% Tween-20, then heated at 85°C in reducing SDS loading buffer before magnetic removal of A/G beads prior to loading the samples (10 % total sample loaded for each brain region) onto 4–12% NuPage Bis-Tris precast gels. After electrophoresis, the proteins were transferred to nitrocellulose membranes. Membranes were blocked in 5% Blotto/PBST for 1 h at room temperature (RT, 25°C). Membranes were incubated overnight at 4°C with HRP-conjugated goat anti-MPO (BD Transduction)(1/3000) for 1 h at RT and washed three times with PBST for 30 min. The blot was developed with ECL reagent and exposed to X-ray film.

2.13 Synaptosome isolation

Crude synaptosomes were isolated essentially as described [65] using Syn-Per reagent (Thermo Fisher) according to the manufacturer's protocol. Two ml of Syn-Per with protease inhibitors was added to 200 mg of brain tissue followed by homogenization using a dounce homogenizer. The homogenate was centrifuged at 1200 × g for 10 min at 4°C to remove nuclei and debris. The supernatant was then centrifuged at 15,000 × g for 20 min at 4°C to

yield the crude P2 synaptosome pellet which was resuspended in Syn-Per at 3–4 μg/μl protein concentration.

2.14 Cellulose acetate filter binding assay

The amount of aggregated insoluble αSyn present in the brain lysates was assessed by cellulose acetate filter binding assay. Synaptosomal preparations were diluted 1/150 volume in PBS pH 7.4 with 1% NP40 and placed on a rotary mixer for 5 h at 4°C, and then a total of 100 mg protein filtered by mild suction through 0.2 μm cellular acetate filters (Whatman), followed by five washes with PBS with 1% SDS. The cellulose acetate strips were then blocked with 5% Blotto, and incubated with LB509 antibody generated against Lewy bodies (1/1000) for 1 h. This antibody recognizes hαSyn but not mαSyn. The membrane was washed in PBST for 1 h and incubated with secondary antibody (goat anti-mouse IgG HRP, 1:10,000) for 1 hr prior to being developed with ECL reagent. Semi-quantitative densitometry of the Western blots was analyzed using Image Studio Lite software (LI-COR 0Biosciences, NE, USA).

2.15 αSyn oxidation in vitro

hαSyn (1 mg/ml) was incubated with hMPO (20 nM), glucose oxidase (GO, 20 ng/ml) and glucose (100 μg/ml) as a source of H_2O_2 and either sodium nitrite (500 μM) or potassium cyanate (340 μM) for 6 h at 37°C. Proteins were fractionated by SDS-PAGE (4%–12%). Proteins were then transferred to nitrocellulose and probed with the respective antibodies: anti-alpha synuclein (1:1,000, BD), anti-nitrated tyrosine (1:1,000, Millipore), anti-carbamylated αSyn (1:1,000, described here). Blots were incubated in 5% Blotto in PBST for 1 h and then incubated in PBST containing 1% BSA with the appropriate antibody for 2 h at RT. The membranes were washed for 1 h in PBST at RT. Membranes were then incubated with HRP-labeled secondary antibodies in PBST + 1% BSA for 1 h. Following this incubation the blots were washed in PBST and then incubated with ECL reagent and exposed to X-ray film. For analysis of αSyn by liquid chromatography tandem MS (LC-MS/MS), samples were treated as above but the gel was stained with Commassie blue and the band containing the αSyn monomer was excised and analyzed for post-translational modifications.

2.16 In-gel digestion and sample preparation for LC-MS/MS analysis

Respective Commassie blue stained protein bands were excised from the gel and destained prior to protein reduction and alkylation. Bands were then digested with trypsin at a final concentration of 25 ng/μl in 50 mM ammonium bicarbonate for 1 h on ice, excess trypsin was removed and gels were digested for an additional 16 h at 37C using a shaking incubator to assure complete digestion. Digested tryptic peptides were transferred to a new tube following an elution process; 200 μl of water added to the gels, sonicated 10 min in water bath and then extracted one time in 5% formic acid, one time in water, four times with 50% acetonitrile in 5% formic acid in water, one time in 70% acetonitrile, and one time in 100% acetonitrile; all extracted peptides were pooled together, vacuum dried and re-dissolved in 20 μl of 0.1% trifluoroacetic acid. Tryptic peptides were desalted and concentrated using a C18 Zip Tip (Millipore). The eluents were then vacuum dried and re-dissolved in 24 μl of LC/MS loading buffer (2% acetonitrile in 0.1% formic acid in water).

2.17 1D LC-MS/MS Analysis

Tryptic digested proteins were subjected to an on-line analysis of peptides by one-dimensional LC-MS/MS. Eight μl of tryptic digested sample was loaded onto the automated Nano LC-LTQ MS/MS (Thermo Scientific) using an Eksigent (SCIEX) Nano 2D LC system, a switch valve, a C18 trap column (Agilent, Santa Clara, CA) and a capillary reverse-phase column (15 cm Magic C18 AQ resin (Michrom)). An ADVANCE low flow Michrom source (Bruker-Michrom) was used to ionize peptides as they elute from the capillary column in a linear gradient from 100% buffer A (2% acetonitrile in water containing 0.1% formic acid) to 40% buffer B (100% acetonitrile in water containing 0.1% formic acid) over 103 min for the total run time of 120 min. Data relevant to the strongest ions above an intensity of 50×10^4 were collected with dynamic exclusion enabled on top 5 precursor and the collision energy set at 35%.

2.18 Protein Identification and data analysis

The LC-MS/MS raw data was submitted to Sorcerer Enterprise v.3.5 release (Sage-N Research Inc.) with SEQUEST algorithm as the search program for peptide/protein identification. SEQUEST was set up to search the target-decoy ipi.Human.v3.73 database containing protein sequences using trypsin for enzyme with the allowance of up to 2 missed cleavages, Semi Tryptic search and precursor mass tolerance of 1.5 amu. Differential search includes methionine oxidation, cysteine carboxyamidomethylation, tyrosine nitration and lysine carbamylation with maximum 3 post translational modification/peptide allowance. The search results were viewed, sorted, filtered, and statically analyzed by using comprehensive proteomics data analysis software, Peptide/Protein prophet v.4.02 (ISB). The minimum trans-proteomic pipeline probability scores for proteins and peptides are both 0.95 and 0.9, respectively, to assure very low error (much less than FDR 2%) with reasonably good sensitivity. The differential spectral count analysis was done by QTools, an open source in-house developed tool for automated differential peptide/protein spectral count analysis and Gene Ontology [66]

2.19 Preparation of antibodies to carbamylated αSyn

Three peptides to carbamylated αSyn were generated containing the modified lysines (homocitrulline) indicated by an asterisk. Peptide #1: aa32-KTK*EGVLYVGSKTK*EGSC-aa47; peptide #2: aa52-VATVAEK*TK*EQVTNVGSC-aa67; Peptide #3: aa73-GVTAVAQK*TVEGAGSGSC-aa87. Peptides were synthesized, purified, and conjugated to keyhole limpet hemocyanin (KLH) by PHD antibodies (San Diego, CA). Polyclonal antibodies against carbamylated αSyn peptides linked to KLH were raised in rabbits. Immunizations were performed by Robert Sargeant (Ramona, CA) using a standard protocol. The collected blood sera were kept frozen at −8 °C until needed. The antibod ies to carbamylated αSyn were purified by affinity chromatography using the αSyn peptides used as immunogens immobilized to cyanogen bromide activated Sepharose® 4B. The resin and columns were prepared according to the product manual. Briefly, serum proteins were passed through the column with the carbamylated αSyn peptides. Absorbed antibody was eluted with 0.1 mol/L glycine-HCl (pH 2.6) buffer and monitored with a spectrophotometer at 280 nm. The resulting immunoglobulin containing fraction was dialyzed against PBS. The

antibodies to carbamylated αSyn were further enriched by affinity chromatography using carbamylated BSA immobilized on cyanogen bromide-activated Sepharose® 4B. The antibodies were eluted as described above. After every chromatography, the specificity of purified antibodies was evaluated by Western blotting.

Carbamylated BSA was prepared by *in vitro* modification of BSA. Briefly, BSA (50 mg/ml) was dissolved in PBS and potassium cyanate (1 mM) in PBS was added to the protein solution. The mixture was incubated at 37°C for various times from 1 h to overnight. Potassium cyanate was removed by extensive dialysis against PBS at 4°C. T he level of carbamylation was evaluated by Western blot and a concentration of carbamylated BSA that corresponded to about 50% carbamylation was used for the column. After an initial evaluation by Western blot the antibody raised against peptide #1 (carbsyn-1) was found to give the best signal and was used for all subsequent experiments. Specificity of carbsyn-1 was evaluated by Western blot comparing carbamylated αSyn (1 mM potassium cyanate) versus non-carbamylated αSyn. In addition, a blocking experiment was performed. A five-fold excess of peptide #1, that was used as the immunogen, was mixed with the antibody and incubated for 30 min at RT. The neutralized antibody was used for a Western blot comparing carbamylated αSyn versus non-carbamylated αSyn.

2.20 Homocitrulline quantification

Quantification of HCit was performed as described [67]. Protein samples were hydrolyzed with a high-throughput low-volume hydrolysis method as described previously [68]. Briefly, protein samples (3 to 20 μg) were placed into Qsert vials (Waters, Vienna) and 10 μl internal standard was added (containing 10 ng $^{13}C_6$-HCit, 10 ng $^{13}C_6$-3-CT, 0.3 μg $^{13}C_6$-tyrosine and 1 μg $^{13}C_6$-lysine). Hydrobromic acid with 0.25% phenol was added to a final concentration of 6 N, vials were flushed with argon, sealed and hydrolyzed at 160°C for 5 min. Afterwards, hydrobromic acid was evaporated in a speedvac. Protein hydrolysates were suspended in 100 μl 0.2 mol/L Li-citrate buffer (pH 2.8) and derivatized with the EZ:fast Kit (Phenomenex, Aschaffenburg, Germany) according to the manufacturer's instructions.

Electrospray ionization MS/MS with online HPLC was used for quantification of HCit and lysine. Calibrations curves were prepared using varying amino acids and homocitrulline levels with fixed amounts of internal standards. The calibration curves had a linearity range from 50 pg – 100 ng for HCit (R2: 0.998 and R2: 0.999) and from 100 ng – 3 μg for lysine (R2: 0.997 and R2: 0.998).

The HPLC column (250×4 mm, AAA-MS HPLC column, Phenomenex, Aschaffenburg, Germany) was equilibrated for 15 min with 100% solvent A at 35°C. Solvent A was 10 mmol/L ammonium formiate in water and solvent B was 10 mmol/L ammounium formiate in methanol. After equilibration, the sample (10 μl) was injected onto the HPLC column at a flow rate of 0.25 ml/min. Compounds were eluted with a discontinuous gradient starting with 83% solvent B for 13 min followed by 68% of solvent B for 4 min. The HPLC column effluent was introduced into an API 2000 triple quadrupole mass spectrometer (SCIEX). Ions were generated by Electrospray ionization in the positive-ion mode with multiple reactions monitoring of parent and characteristic daughter ions. Following transitions were monitored indicated by their mass-to-charge ratio (m/z): m/z 318→127 for HCit; m/z

361→170 for lysine. Following mass spectrometry analysis, the generated calibration curves were used to quantify HCit and lysine.

2.21 In Situ Hybridization (RNAscope)

For *in situ* hybridization experiments mice were sacrificed, perfused with ice cold PBS and the brains removed and transferred to 4% PFA in 1 × PBS and incubated at 4°C overnight. The next day the brains were removed from the PFA and washed in 1 × PBS. The brains were paraffin fixed and processed as described above.

RNAscope *in situ* hybridization was used to detect single RNA transcripts according to the manufacturer's protocol (Advanced Cell Diagnostics). The probe used in this study was hMPO (cat no.469561).

The tissue sections were treated with RNAscope Protease IV at room temperature for 30 min and then the slides were washed in 1 × PBS. Probes were added to the appropriate sections. Sections were then incubated at 40°C for 2 h in a humidified incubator followed by treating them with the RNAscope Fluorescent Detection Reagents Kit solutions AMP 1_FL, AMP 2-FL, AMP 3-FL, and AMP 4-FL. The sections were washed between each incubation according to the manufacturer's recommendations. Sections were then treated with DAPI and a coverslip applied. The slides were stored in the dark at 4°C until analyzed. In microscopic images, each punctate dot represents a single RNA molecule.

2.22 Quantitative RT-PCR (qPCR)

RNA was isolated using Trizol as described by the manufacturer (Life Technologies). cDNA was prepared using the High-Capacity cDNA Reverse transcription Kit (Life Technologies). Quantitative qPCR was performed using an Applied Biosystems 7900HT TaqMan machine (Applied Biosystems, Foster City, CA). The qPCR was run at 50°C for 2 min, 95°C for 10 min followed by 40 cycles of 95°C for 0.15 min and 60°C for 1 min. The following TaqMan gene expression primers were used with TaqMan gene expression master mix (Life Technologies): mouse glyceraldehyde-3-phosphate dehydrogenase (GAPDH), (4326317E), mouse beta 2 microglobulin (Mm00437762_m1), mMPO, (Mm00447886_m1), hMPO (Hs00165162_m1), mαSyn (Mm01188700_m1), and hαSyn (Hs00240906_m1). Samples were run in duplicate and all experiments were repeated at least three times. Relative expression levels were determined by the difference between threshold cycles normalized against mouse GAPDH as internal control (the $2^{\Delta\Delta}$ Ct method) [69]. Group differences were evaluated by ANOVA. GraphPad Prism (v8) (GraphPad Software Inc., San Diego, CA) was used for all calculations and for the preparation of graphs. All values are expressed as the mean ± SEM. A p value of 0.05 or below is considered significant.

2.23 Primary neuronal culture

Primary neuronal cultures were isolated essentially as described [70, 71]. Briefly, pregnant female mice were collected from timed matings, and embryos were harvested from wild-type (WT) and hMPO-A53T animals at embryonic day 17. Primary cortical and hippocampal neurons were obtained by microdissection of the cerebral cortex from embryos using a stereomicroscope and dispersed by digestion in trypsin-EDTA (0.05%) and DNAse I

(400 u/ml) for 30 min at 37°C followed by trituration in DMEM. Embryonic tissue was also collected at harvesting and processed for genotype analysis by DNA extraction and PCR using probes specific for hMPO and A53T-αSyn. WT and hMPO-A53T neurons from individual embryos were maintained separately. Neurons were plated and maintained on poly-d-lysine-coated coverslips or culture dishes in Neurobasal Plus medium supplemented with B27, and penicillin/streptomycin. Medium was changed every 3 d (half of the medium was replaced). Cells were harvested around day 10 – 14. At least three separate experiments were performed for each genotype.

2.24 Protein measurements

Protein concentrations were measured by the BCA protein assay (Pierce) with BSA used as the calibrator.

2.25 Statistical analysis

All experiments were performed blind and in duplicate or triplicate. All values are expressed as the mean ± S.E.M. Statistical differences were considered significant at $P < 0.05$ level. All analyses were performed using GraphPad Prism v8. Behavior data were analyzed using a one-way analysis of variance (ANOVA) or Student's t-test.

3. Results

3.1 hMPO transgene is expressed in neurons in the A53T-αSyn mouse model

To investigate the potential effects of MPO expression in brains of a mouse model overexpressing αSyn, we crossed our hMPO transgenic mouse to a model expressing the hαSyn gene with the A53T mutation driven by the human Thy-1 promoter [49, 50]. A number of A53T αSyn models driven by different promoters have been generated and while none represent a perfect model of PD, these models have provided valuable information as to the pathological consequences of αSyn oxidation and aggregation. While PD is characterized by the selective loss of dopaminergic neurons in the SN, this selective loss is not observed in most A53T mouse models. A53T models typically exhibit widespread expression of A53T αSyn in various subsets of neurons in the CNS with neuropathology preferentially occurring in brain stem and spinal cord. For this study we chose to use the A53T mouse model B6.Cg-Tg(THY1-SNCA*A53T)M53Sud/J (Jackson 008135) which has been previously well characterized and found to simulate some aspects of PD [50, 51]. This model develops early motor impairment progressing to fatal age related paralysis and models neurological aspects of PD including SN degeneration with loss of ~60% of SN dopaminergic neurons as well as thinning of cortical layers and some dystrophy in hippocampal neurons [50, 51]. We crossed this A53T model to our hMPO transgenic (hMPO-A53T). The hMPO model was created by microinjection into C57Bl/6J eggs of a 32-kb restriction fragment from a BAC clone containing the hMPO gene with several kb of 5' and 3' flanking sequences [29]. In our studies these hMPO-A53T mice develop motor impairment that is quantifiable by 6 weeks of age, while onset of late stage hind limb paralysis and death occurs around 9 months of age.

Immunostaining of brain sections from hMPO-A53T mice at ages from 6 to 9 months showed MPO presence in subsets of neurons in many regions of mouse brain, notably cortical neurons (Fig. 1A), hippocampal CA2/3 neurons (Fig. 1B), midbrain (Fig. 1C), cerebellum (Fig. 1D), and spinal cord (Fig. 1E). We did not detect significant mMPO immunostaining in these brain regions in the A53T mice (Fig. 1F–J). Those sections are counterstained with nuclear fast red to allow visualization of the cellular architecture.

We identified the MPO positive cells as neurons by costaining for MPO and the neuron dendritic marker microtubule-associated protein (MAP2) in hippocampus and cortex (Fig. 1K,L). MPO localized to the cell body while MAP2 localized in the neurites. The separate green and red channels are below the merged panel (Fig. 1K,L) to show examples in which the green projections contact the red neural soma (arrows). We also found costaining for MPO and the neuronal marker NeuN in the cortex (Fig. 1M,N) in the hMPO-A53T mice. Quantitation of the percentage of cortical neurons expressing both MPO and NeuN in hMPO-A53T and A53T brain shows significant numbers of positives in the hMPO-A53T brain but not in A53T due to lack of significant mMPO expression (Fig. 1 O). From the results we conclude that in this hMPO-A53T model, hMPO can be expressed in neurons.

3.2 MPO expressed in hMPO-A53T brain is the secreted 90 kDa proMPO form

In myeloid precursor cells, the MPO protein is expressed as a 90 kDa precursor which is proteolytically cleaved in the ER to generate the 59 kDa heavy chain and 15 kDa light chain. In a series of events the protomers are covalently bound through a heme group and two protomers are subsequently linked via a disulfide bond between the two heavy chains (reviewed in [72]). In promyelocytes the MPO is trafficked to azurophilic granules and when neutrophils phagocytose microbes, the MPO containing vesicles fuse with the phagosome vesicle to release MPO to the interior, whereupon MPO reacts with Cl-to generate HOCl and other microbicidal oxidants. The MPO precursor can also enter the secretory pathway leading to extracellular release (reviewed [72]). Our recent study found that the MPO cDNA transfected into cell lines can be expressed in breast cancer cell lines as the 90 kDa monomer which enters the secretory pathway and is released from cells or processed to the heavy and light chains and trafficked to the lysosome [56]. To investigate the form of hMPO produced by cells in the brain, we made extracts from four mice of MPO-A53T and four mice of A53T genotype, The brains were cut into three similar sized regions including cortex/hippocampus (C), cerebellum/brainstem (including pons, medulla, spinal cord)(CB), and the remainder as midbrain (MB) (including thalamus, striatum, substantia nigra). Extracts were prepared and protein concentrations determined by BCA reagents to ensure equal protein concentrations for immunoprecipitations. We immunoprecipitated MPO using a rabbit anti-MPO antibody (Dako) and magnetic protein A/G beads (Dyna beads), followed by fractionation of the proteins by SDS-PAGE and probed by Western blot with an HRP-conjugated affinity purified goat anti-MPO antibody (R&D systems). These Western blots show the 90 kDa proMPO as the predominant form of MPO in the hMPO-A53T brain. There was little to no 59 kDa MPO heavy chain detected in these regions. Interestingly, the highest concentration of MPO 90 kDa proMPO is in the cortex, with approximately half as much in midbrain, and little in cerebellum/brainstem (Fig. 2A, lanes 1–3). Extracts of the A53T brains lacking the hMPO transgene showed no proMPO and no 59 kDa MPO heavy

chain (Fig. 2, lanes 5–7). As a control, the protein A/G beads alone did not pull down proteins detected by goat anti-MPO (Fig. 2A, lane 4, pag). The Western blot was probed for rabbit IgG heavy chain as a loading control to detect DAKO anti-MPO antibody (IgG HC).

In panel B, the same immunoprecipitation procedure was carried out with brain extracts from hMPO-Syn61, which expresses hMPO and the human wild-type αSyn gene, hMPO-APP23, which expresses hMPO and the human amyloid precursor protein, as well as extracts of WT mouse bone marrow cells. The 90 kDa MPO precursor was the predominant form in hMPO-A53T (Fig. 2B, lane 1), hMPO-Syn61 (Fig. 2B, lane 4), and hMPO-APP23 (Fig. 2B, lane 2), while the 59 kDa heavy chain was predominant in mouse bone marrow cells (Fig. 2B, lane 3). The Western blot was probed for rabbit IgG heavy chain as a loading control to detect DAKO anti-MPO antibody (IgG HC).

These findings indicate that neurons are less able than myeloid precursor cells to process the MPO precursor to the heavy and light chains. It is important to note that the MPO precursor has the same enzymatic activity as the mature tetramer MPO enzyme [73], and because the precursor is the secreted form, this raises the possibility that MPO could be secreted from neurons resulting in oxidative damage to neighboring cells.

We quantified the level of MPO in the brains of the humanized mouse MPO-A53T, along with A53T, C57Bl/6 wild type and in PD SN by ELISA (Fig 2C). We determined that in both the humanized MPO mouse and in the MPO-A53T mouse brains there was between about 2000 and 1700 pg/mg protein, respectively (Fig. 2C). In the A53T and the C57Bl/6 mouse brains there were 6 fold lower levels of MPO protein (250 pg/mg) as determined by this assay. Interestingly, we determined that PD SN also contained MPO protein (between 1000 and 1500 pg/mg protein). We then performed immunoprecipitation experiments with extracts from human PD SN tissue (Fig. 2D). The results show the presence of the proMPO 90K protein in human PD SN, comigrating with the 90K band in cortical extracts from MPO tg and MPO-A53T. The PD SN extract also showed the 55–59 kDa MPO heavy chain and a 70 kDa band which may be a processing intermediate [56]. Immunoprecipitation of extracts of A53T or wildtype brains lacking the hMPO tg showed no proMPO or processed MPO bands.

3.3 MPO mRNA is expressed in neurons in the hMPO-A53T model

To validate the immunodetection of hMPO protein in neurons in the hMPO-A53T brain, we looked for the presence of MPO mRNA by RNAscope *in situ* hybridization [74]. This highly sensitive method enables detection of single mRNA molecules as distinct puncta in high-resolution confocal images. Also, MPO-positive neutrophils and monocytes are not detected as these cells store MPO protein but do not express MPO mRNA. Using probes specific for hMPO mRNA, we detected respective mRNAs in puncta (red) in hippocampal CA2 neurons (Fig. 3A), seen more distinctly as individual puncta in a single enlarged neuron in a confocal image (63x) (Fig. 3B). MPO mRNA puncta were also detected in cortical neurons (Fig. 3C), seen more distinctly in several neurons magnified in the inset. MPO mRNA was similarly detected in a lower magnification image of dentate gyrus neurons (blue HRP substrate) (Fig. 3D).

To compare the relative level of hMPO and mMPO mRNA expression in the hMPO-A53T mouse model, qPCR analysis was performed. mRNA was isolated from whole mouse brains, and cDNA was prepared from 4 to 6 biological replicates of hMPO transgenic, hMPO-A53T, or WT C57Bl/6 at ages between 6 to 8 months. TaqMan qPCR was performed using primers specific for hMPO or mMPO, and the results were normalized against mouse GAPDH. The hMPO transgenic or hMPO-A53T mice contain both the hMPO transgene (1 copy) and WT mMPO (2 copies). The relative fold change in hMPO and mMPO mRNA levels were determined by the $2^{\Delta\Delta}$ Ct method [69] and are shown in Fig. 3E and 3F. hMPO and mMPO mRNA levels were relatively high in bone marrow from the hMPO transgenic model (both Ct 25) (Fig. 3E, lanes 1 and 2), equivalent to control GAPDH mRNA levels (not shown). In hMPO brain, hMPO and mMPO mRNA levels were relatively low compared to bone marrow (Fig. 3E, lanes 3–6), and so these four columns are expanded in Fig. 3F. In brain, hMPO mRNA levels decreased by ~100 fold (Ct 31.8), a moderate expression level as compared to bone marrow. In brain, mMPO levels fell more sharply from Ct 25 to Ct 37.6 (~ 6000 fold) (Fig. 3F, lane 6), indicating very low to nondetectable expression. Interestingly, in the presence of A53T, hMPO mRNA expression was slightly higher (Ct 31.3)(lane 3) than in hMPO brain lacking αSyn (Ct 31.8) (lane 4), suggesting αSyn overexpression might promote hMPO expression. This was not true for mMPO expression which was slightly lower in hMPO-A53T brain (Ct 39) (lane 5) than hMPO brain (Ct 37.6)(Fig. 3, lane 6). These findings show that the hMPO transgene is expressed at significant levels in brain tissue, while the mMPO gene is expressed at very low to nondetectable levels. ($***p < 0.005$ for hMPO vs mMPO (Fig. 3, F,G).

3.4 hMPO protein and mRNA is expressed in cultured embryonic neurons

As further evidence of hMPO expression in neurons, we isolated neurons from day 17–18 hMPO transgenic embryonic brain cortex and cultured these for 10–14 days *in vitro* to obtain neurons with dendrites and axonal processes that immunostain for the neuronal marker GluR1 (glutamate receptor 1). In these embryo derived neurons (Fig. 3H–J), hMPO protein was immunodetected in the soma and neuronal processes (Fig. 3I) along with GluR1 (Fig. 3H, Merged J). To determine the relative levels of hMPO and mMPO mRNA expression in these neurons, we carried out qPCR and found levels of hMPO mRNA expression (Ct 30) similar to that seen in adult hMPO-A53T brain (Fig. 3G, lane 7). Again, mMPO mRNA levels were extremely low (Ct 38) (Fig. 3G, lane 8) and in some cases undetectable. The absence of significant levels of mMPO mRNA in neurons is consistent with our finding of low to undetectable levels of mMPO protein in the brain (Fig. 1, F–G). We conclude that the hMPO gene is expressed in neurons in hMPO transgenic or hMPO-A53T brain, while mMPO gene expression is low to nondetectable in brain or neurons.

3.5 hMPO transgene expression in neurons in the A53T-αSyn mouse model is associated with increased nitration of αSyn.

Immunostaining of brain sections from symptomatic hMPO-A53T mice at ages from 6 to 9 months showed MPO expression to be often associated with unhealthy appearing neurons. In midbrain neurons, MPO expression (black) was observed in dystrophic neurons that costained for αSyn (Syn505, red)(Fig. 4A, with boxed area enlarged in Fig. 4B). Monoclonal antibody Syn505, raised against nitrated αSyn, detects both nitrated αSyn and

native αSyn [57]. Syn505 is also suggested to recognize conformational variants of αSyn that are enhanced by the A53T mutation, such as αSyn fibrils in pathological inclusions [75].

Cortical neurons expressing MPO (red) in the soma also costained for nitrated tyrosine (Millipore rabbit, green) in neural processes (Fig. 4C). Single channel green imaging (Fig. 4C') suggests more intense nitrated tyrosine staining in processes than in soma. MPO can generate nitrating intermediates leading us to further investigate the presence of nitrated αSyn in MPO expressing neurons. To this end, we used another monoclonal antibody, nSyn14 [59], which was raised against nitrated αSyn and selectively recognizes nitrated αSyn but not native αSyn, and recognition requires nitrated tyrosine at position 39, a modification increased in PD [76]. nSyn14 detects subsets of hippocampal neurons in CA2/3 (red)(Fig. 4G,H) that also express hMPO (green) (Fig. 4E,F merged images in I and J) in the hMPO-A53T mouse. At higher magnification, punctate/granular MPO immunostaining (green) and nSyn14 (red) was detected in neurons (Fig. 4L). Single channel red staining is also shown for nSyn14 (Fig. 4K). Quantitation of the percentage of hippocampal neurons in CA2/3 region that costain for MPO and nSyn14 are shown for MPO A53T (23 %) and A53T (3 %) (Fig. 4D). The low level of costaining in A53T reflects the absence of significant mouse MPO expression. We conclude that hMPO is expressed in neurons containing nitrated αSyn, as well as nitrated tyrosine.

3.6 Increased nitrated tyrosine in hippocampus and cortex in hMPO-A53T relative to A53T brain

Increased staining of nitrated tyrosine (nitroTyr) was detected in the pyramidal neurons of the CA2/3 region of hippocampus of hMPO-A53T mice (Fig. 5A) (boxed region enlarged in Fig. 5B) as compared to A53T (Fig. 5C) (boxed region enlarged Fig. 5D). The results from immunohistochemical staining (Fig. 5A–D) were quantified in Fig. 5 I. Similarly, we detected increased levels of nitroTyr in the cortex of MPO-A53T (Fig. 5E) (boxed area enlarged in Fig. 5F) as compared to A53T (Fig. 5G) (boxed area enlarged in Fig. 5H). The results from immunohistochemical staining (Fig. 5E–H) were quantified in Fig. 5J. These findings show that hMPO transgene expression correlates with increased levels of nitroTyr in the hippocampus and cortex of the hMPO-A53T model.

3.7 Colocalization of MPO and HOCl-modified epitopes in hMPO-A53T cortical neurons.

The next series of experiments were performed to reveal whether MPO colocalizes with HOCl-modified epitopes in cortical regions using monoclonal antibody 2D10G9 that was raised against HOCl-oxidized/modified epitopes, which are exclusively generated by the MPO-H_2O_2-C^- system [60, 61]. (Fig. 6A–E). MPO was bound by DAKO anti-MPO and detected with fluorescent green secondary antibodies to rabbit IgG (A, AlexaFluor 488). HOCl-modified epitopes/proteins bound by 2D10G9 were detected with fluorescent red secondary antibodies to mouse IgG (B, AlexaFluor 594), Merged image (C) shows many neurons have small regions that colocalize (yellow) for MPO and HOCl-modified epitopes. The neuron in the central box in panel C is enlarged in left inset in A-C. The upper box in panel C is enlarged in panel D showing the speckled green pattern of MPO immunostaining suggestive of endosomal vesicles. Panel D also shows a neuron with unstained nuclear area

(arrowhead) and an adjacent area of colocalization (yellow) for MPO and HOCl-modified epitopes (arrow). As a control, use of the secondary antibody in the absence of 2D10G9 primary antibody resulted in lack of staining (Fig. 6E). We also compared immunoperoxidase staining of 2D10G9 antibody of MPO-A53T versus A53T cortical neurons (Fig. 6F,G). Peroxidase substrate detection of 2D10G9 revealed higher levels of HOCl modified epitopes in MPO-A53T than A53T cortex. Quantification of the relative immunostaining density is shown in Figure 6H. These findings provide evidence that MPO expression coexists in cells exhibiting HOCl modified epitopes.

3.8 Increased carbamylated lysine in hMPO-A53T compared to A53T brain

We next set out to investigate whether carbamylation occurs in hMPO-A53T and A53T brain. In order to detect carbamylated lysine, we generated sequence specific rabbit polyclonal antibodies against carbamylated peptides of αSyn, and then affinity purified the antibodies against carbamylated BSA to remove contaminating antibodies to native αSyn. A low magnification (20x) image shows the merged image with immunostaining against carbamylated αSyn (green) and MPO (red) in pyramidal neurons of the CA3 region (Fig. 7A). The boxed area is further enlarged to show colocalization (yellow) of MPO (red) and carbamylated αSyn (green) in a subset of neurons (63x) (Fig. 7B). Single channel images show immunostaining for either carbamylated αSyn (Fig. 7C) or MPO (Fig. 7D). Immunostaining was performed with the anti-carbamylated lysine antibodies to compare the relative numbers of positive neurons in the CA3 region in MPO A53T versus A53T hippocampus (Fig. 7E,F). We analyzed five brains of each genotype, using three sections from each brain, and counted immunopositive neurons in four regions of CA3 in each section. Quantitation showed a significant increase of carbamylated lysine positive neurons in the CA3 region of hMPO-A53T brain versus A53T brain (Fig. 7G). To quantitate the amounts of carbamylated lysine, extracts were prepared from hMPO-A53T and A53T brains and analyzed by mass spectrometry to confirm significantly higher levels of HCit (carbamylated lysine) in the hMPO-A53T brains as compared to A53T brains (Fig. 7H).

A characterization of the antibody carbsyn-1 was undertaken to verify the specificity of the antibody. αSyn was treated with 1 mM potassium cyanate and 0.2 micrograms or either carbamylated αSyn or αSyn was fractionated by gel electrophoresis and a Western Blot performed using the carbsyn-1 antibody (Fig 7 I lane 1 and 2). The carbsyn-1 antibody only recognized the carbamylated αSyn (lane 1) but not αSyn (lane 2). As a control the same amount of carbamylated αSyn and αSyn was fractionated by gel electrophoresis and a Western blot performed using an antibody that recognizes αSyn (BD) (Fig 7 I lane 3 and 4). The antibody to αSyn recognized both the carbamylated αSyn and the αSyn although the signal from the carbamylated αSyn was weaker than that from the αSyn. This is likely due to the carbamylation of αSyn interfering with the recognition by the antibody. Finally, we performed an antibody neutralization experiment by incubating the carbsyn-1 antibody with the peptide (peptide #1) used to generate the antiserum. Once the carbsyn-1 antibody was neutralized with the peptide the antibody recognized neither carbamylated αSyn nor native αSyn (Fig 7 I lane 5 and 6).

3.9 MPO nitrates and carbamylates αSyn in vitro resulting in dimers and oligomers

Nitration and oxidation of αSyn is associated with dimerization and aggregation, such as dityrosine crosslinking leading to αSyn oligomers in PD [77, 78]. Dimerization of αSyn could also impair synaptic vesicle fission during clathrin mediated vesicle recycling [79]. Thus, the observed impairment of motor abilities in the hMPO-A53T model could be related to nitration/oxidation of αSyn leading to dimers and oligomers. To examine the ability of MPO to promote αSyn nitration, dimerization and oligomerization, purified recombinant αSyn was incubated with MPO, GO and glucose as a source of H_2O_2 (to generate the MPO-H_2O_2 system) and nitrite (Fig. 8A, lane 2), or in the absence of the MPO-H_2O_2 system and nitrite (Fig. 8A, lane 3), followed by fractionation by SDS-PAGE and Western blot analysis using antibodies against nitrated tyrosine (Millipore). In the presence of MPO-H_2O_2 system and nitrite, the 3-nitrotyrosine antibodies detected nitrated αSyn monomer, dimer, trimer, and higher order oligomers (Fig. 8A, lane 2). These findings show that MPO in the presence of H_2O_2 and nitrite generated nitroTyr residues and probably also *o,o'*-dityrosine crosslinks in αSyn to give rise to dimers, trimers, and oligomers, consistent with an earlier study [80].

Carbamylation represents an alternative route by which MPO can promote protein adduct formation [81]. MPO reacts with thiocyanate (SCN^-) to generate cyanate which carbamylates lysine residues to form HCit [82]. αSyn was incubated with MPO-H_2O_2 system in the presence of SCN^-, then subjected to SDS-PAGE and immunoreactive bands were identified by Western blot using monoclonal antibodies to αSyn (BD transduction). The antibodies detected monomers and dimer formation (arrow), but no higher order multimers (Fig. 8B, lane 5), in contrast to the dimers and higher order oligomers created with the MPO-H_2O_2 system in the presence of nitrite (Fig. 8B, lane 6). This shows that carbamylation driven by MPO-H_2O_2 can lead to αSyn dimerization which could contribute to pathological αSyn conformations.

3.10 Mass spectrometry of αSyn monomers identifies sites of nitrotyrosine and carbamylated lysine

The sites of nitration and carbamylation of αSyn were identified by LC-MS/MS. The monomeric αSyn band was isolated from the gel after αSyn had been incubated with the MPO-H_2O_2 system and either nitrite or SCN^-. The nitrated amino acids (red) included $Tyr^{39,\ 125\ and\ 133}$ (Fig. 8C). Previously, it was reported that treatment of hαSyn with peroxynitrite ($ONOO^-$) followed by trypsin digestion and analysis by mass spectrometry identified $Tyr^{39,\ 125,\ 133,\ and\ 136}$ as being nitrated [80]. We did not observe nitration of Tyr^{136}. This may be due to the conformation of αSyn allowing peroxynitrite but not MPO-generated oxidants to nitrate Tyr^{136}. A preference for MPO-mediated nitration versus peroxynitrite mediated nitration was also observed in a study examining the nitration of apoAI [83]. The position of the nitrated Tyr residues on the structural model of αSyn is shown (Fig. 8D).

When SCN^-/H_2O_2/MPO treated αSyn monomer was analyzed by LC-MS/MS to identify carbamylated lysines, we observed that Lys6, $^{34,\ 46,\ 58,\ 60,\ and\ 80}$ were modified (Fig. 8C). Interestingly, there were 9 Lys residues that were not carbamylated, which again may reflect the conformation of αSyn that determines the accessibility of Lys residues to MPO

generated oxidants. The position of the carbamylated Lys residues on the structural model of αSyn is shown (Fig. 8D).

3.11 Increased levels of detergent insoluble αSyn in hMPO-A53T brain compared to A53T

The cellulose acetate filter trap assay is a means to compare the amounts of insoluble αSyn aggregates in hMPO-A53T versus A53T brain. Crude synaptosomal fractions were prepared from four hMPO-A53T and four A53T brains from mice at later stage disease with partial paralysis, followed by filtration through cellulose acetate filters with pore sizes allowing retention of insoluble aggregates. Preparation entails dounce homogenization followed by low speed centrifugation to remove nuclei and debris, followed by higher speed centrifugation to enrich for synaptosomes (pre- and post-synaptic termini). The pellets were resuspended and protein concentrations of the synaptosomal pellets were determined by BCA assays to allow equivalent amounts of total protein to be used for filtration (100 μg). The crude synaptosomes were resuspended and incubated for 1 h in PBS with 1% NP40 and then filtered by mild suction through 0.2 μm cellular acetate filters, followed by four washes with PBS plus 1% SDS. The cellulose acetate strips were then incubated with monoclonal antibody LB509 which was generated against Lewy bodies and recognizes hαSyn but not mαSyn. Binding of LB509 to the strips was detected by HRP-conjugated anti-mouse IgG (Fig. 8E). Quantitation of band intensity was performed with Image Studio Lite software (Fig. 8F) revealing significantly more detergent insoluble αSyn in hMPO-A53T brain as compared to A53T.

3.12 MPO expression exacerbates motor impairment in the hMPO-A53T mice

To determine if hMPO expression affects motor abilities in the hMPO-A53T model, we carried out standard motor behavior tests. Mice heterozygous for the hMPO and A53T transgenes were used in the behavior assays to ensure equivalent copy number of each transgene. The single copy hMPO transgene is located on the X chromosome. In heterozygous female mice, due to random X chromosome inactivation, half of the neurons lack the hMPO transgene, while all neurons in male mice will have one active hMPO transgene. For this reason, male mice were used in the behavior studies shown. The female hMPO-A53T mice were also tested and exhibited the same pattern of motor deficits as males, but the effects were less significant, likely due to hMPO expression in only 50% of neurons.

The accelerating Rotarod tests balance, coordination, muscle strength, and stamina as the mice are required to maintain balance on a rotating bar that accelerates from 2 to 20 RPM over a period of 300 s. Mice at ages between 45 and 60 days were tested on the rotarod with three consecutive tests of 300 s with a 5 min rest interval (Fig. 9A). C57Bl6/J mice (WT) (white bar) or the hMPO mice (MPO)(red stripe) were in most cases able to remain on the rotarod for the entire 300 s resulting in a mean latency to fall of 275 s. The A53T mice (grey bars) were less able to maintain balance resulting in a latency to fall of 206 s, while the hMPO-A53T mice (red bars) were the least able to maintain hold with a mean latency of 151 s on trial 1. These findings show that the hMPO transgene exacerbates the motor impairment of the A53T mice at these early ages. Importantly, the hMPO transgene had no effect on

motor abilities in the absence of the A53T gene (compare WT and hMPO), indicating that hMPO synergizes with αSyn to exacerbate αSyn mediated motor impairment.

The wire hang is a method to test grip strength, stamina, and neuromuscular dysfunction (Fig. 9B). The mice are required to support their weight inverted on a cage top for up to 60 s for three consecutive tests with 60 s rest intervals. In most cases, wild type mice (WT) or hMPO (MPO) mice easily maintained grip through the three 60 s trials (mean latency to fall of 56 s). The A53T mice (grey) fell at a mean of 37 s on the first trial and earlier on succeeding trials. The hMPO-A53T (red) fell even earlier at a mean of 19 s on trial 1, and earlier on successive trials. Again the hMPO transgene had no effect on grip strength in the absence of the A53T transgene, demonstrating that hMPO and αSyn synergize to exacerbate motor impairment.

The balance beam is another test of balance and motor impairment (Fig. 9C). Mice are required to traverse a dowel (1 m) with diameter of 1 cm. WT or hMPO mice traverse the beam in less than 10 s while the A53T mice required a mean of 18 s and the hMPO-A53T mice crossed in mean 34 s. Again, there was no effect of the hMPO transgene alone indicating a functional interaction between hMPO and αSyn to increase motor impairment at these early stages of αSyn mediated damage. As further indication of the negative impact of MPO oxidants in association with αSyn, survival curves show that hMPO expression in the A53T model leads to earlier onset of end stage paralysis (Fig. 9D). Based on these findings, we conclude that hMPO expression in neurons leads to greater impairment of motor abilities in the A53T model.

3.13 Accumulation of nitrated αSyn in hippocampal CA2 region of hMPO-A53T brain

We hypothesized that nitration and oxidation of αSyn by MPO could worsen αSyn misfolding and aggregation associated with synucleinopathy in PD. Protein misfolding can provoke the unfolded protein response (UPR) which leads to induction of ATF4, leading to production of cleaved caspase-3 and CHOP, resulting in apoptosis. This led us to look for presence of ATF4 and these downstream UPR components in the hMPO-A53T brain. We observed robust ATF4 expression in CA2 dendrites extending into an intense accumulation of αSyn aggregates (Fig 10 A, green, arrow, higher magnification in Fig 10 B). Recent studies with human PD/DLB brain and mouse models have implicated hippocampal CA2 region with greater and earlier αSyn pathology, as well as problems with social recognition memory [86] and cognitive impairment [87–89]. We noted that the accumulation of αSyn was localized at the terminus of CA2 apical dendrites in the stratum lacunosum moleculare (SLM) which receives synaptic input from axons projecting from the entorhinal cortex layer II (EC II) [90, 91]. Because αSyn is primarily localized to presynaptic axon terminals, the αSyn aggregates in the SLM may be present in presynaptic terminals of EC II axons in contact with CA2 dendrites. These CA2 dendrites contained high levels of ATF4 transcription factor (Fig 10 A, red, arrow, enlarged in Fig 10 B). Confocal images (Fig 10 C, with insets enlarged in Fig 10 D and 10 E) show more distinctly the CA2 dendrites immunostained for ATF4 (red) extending into the region of granular αSyn (green). Fig 10 D shows CA2 dendrites containing vesicular ATF4 (red) crossing the mossy fiber tract (MF) of axons from the dentate gyrus (DG) immunostained by Syn505 (Fig 10 D, green). Fig 10 E

shows granular αSyn (green) in potential EC II axon terminals alongside ATF4-positive CA2 dendrites (red). Note the greater size of αSyn aggregates/synaptic terminals in the SLM (Fig 10 E) as compared to αSyn puncta in the MF tract (Fig 10 D), suggesting larger αSyn assemblies or aggregates in the SLM. This ATF4/αSyn505 CA2 pattern was also present but less intense in the A53T model lacking the hMPO transgene (Fig 10 F), as well as the hMPO-Syn61 model which overexpresses the wild type human αSyn gene (Fig 10 G), and in the human αSyn model driven by the PDGF promoter (Fig 10 H) [52]. In the A53T and Syn61 models, the αSyn transgene is driven by Thy1 promoter while the PDGF-αSyn transgene is driven by the PDGF promoter, indicating that this expression pattern is not specific to Thy1 promoter. We also examined the MSA model in which αSyn is driven by the myelin basic protein (MBP) promoter to be expressed in oligodendrocytes [55], and we observed weaker ATF4 expression in CA2 dendrites but no αSyn aggregates in the SLM (Fig 10 I), indicating this accumulation requires αSyn expression in neurons. Finally, wild type brain lacked this pattern of ATF4 expression and αSyn deposition in CA2 (Fig 10 J), indicating this pattern is associated with human αSyn overexpression.

Because ATF4 expression can be induced by ER stress and the UPR, we looked for evidence of UPR mediators downstream of ATF4 [92]. ATF4 upregulates expression of the proapoptotic transcription factor CHOP which we detected in CA2 soma (Fig 10 M, red). CHOP is mainly induced by ER stress and its downstream effects include activation of caspase-3 which was also detected in CA2 soma (Fig 10N, red). MPO mRNA was detected in CA2 soma by RNAscope (Fig 3) and MPO protein was detected by immunostaining (Fig 10 L, red). Consistent with these stress indicators, hematoxylin and eosin staining showed a high number of dystrophic pyknotic condensed neurons in CA2 (Fig 10 K). Examination of a low power image of the hippocampus shows ATF4 to be present in pyramidal neuron soma in CA2 as well as CA3, but ATF4 expression in apical dendrites (AP) was limited to CA2 (Fig 10 O). To identify the ATF4 staining region as CA2, we obtained confocal images showing colocalization of ATF4 (red) (Fig 10 Q) and RGS14 (Fig 10 R), a specific marker of CA2 neurons, shown in the merged image (Fig 10 P). Together these findings provide evidence that in these αSyn overexpressing models of PD, there is a marked accumulation of αSyn aggregates/granules in the SLM of the CA2 region, possibly associated with synaptic termini of EC II axons, and associated with markers of ER stress and apoptosis in the CA2 neurons. This raises the possibility that MPO-oxidized αSyn aggregates in the CA2 SLM could contribute to neuropathology associated with cognitive impairment or social recognition memory in PD.

3.14 MPO is expressed in dystrophic melanized neurons in human PD substantia nigra

Based on results obtained with the hMPO-A53T mouse model, we examined sections of human PD SNpc to determine if MPO might be expressed in neurons or other cell types. Fixed tissues from PD and aged control SNpc were provided by the Harvard Brain Tissue Resource Center and University of California Neurosciences Department. Immunohistological analysis was performed on eight PD cases and eight aged controls. For each SN sample, a minimum of three paraffin sections, spaced by five sections, were analyzed. For each section, we carried out immunohistological staining on four areas of the SN. Representative images are shown in figure 11. We observed MPO immunostaining

(Dako, rabbit) in some neuromelanin positive neurons in PD SNpc in Fig. 11A in which arrowheads indicate the tract of melanized neurons. The neuromelanin tract is more visible in a control SNpc paraffin block (arrow, Fig. 11B). The boxed area of Fig. 11A is enlarged to show MPO immunostaining (black) in neurons (Fig. 11C), with some neurons further enlarged to show the darker MPO immunostain (Fig. 11D) compared to neuromelanin alone (Fig. 11E). This is the first report of MPO expression in neurons in PD SNpc. There was little MPO detected (black) in melanized neurons in control aged SNpc (Fig. 11F and enlarged in 11G). MPO was immunodetected (black) in melanized neurons in early stage PD (Fig. 11H, enlarged in 11I) and MPO immunoreactivity was further increased in SNpc neurons from more advanced PD (Fig. 11J, enlarged in 11K) where some MPO-positive neurons exhibited a fibrillar dystrophic appearance. Within the region containing the SNpc but outside the melanized tract, MPO was also detected in neurons with different morphology, smaller and triangular with neurites as shown at low magnification (Fig. 11L) and enlarged (Fig. 11M), indicating MPO expression also occurs in other neuronal subsets. The percent of melanized neurons containing MPO in the melanized tracts were determined by counting neurons in a minimum of three sections from eight PD and eight normal control SN, with 4 areas imaged per section (Fig. 11 N).

3.15 MPO is expressed in neurons containing aggregates of nitrated αSyn in human PD substantia nigra

We next analyzed SNpc brain sections from the eight PD cases and eight aged controls by confocal immunofluorescence staining for MPO (red) and αSyn (green). High resolution confocal microscopy revealed the robust presence of MPO in vesicles surrounding αSyn aggregates in SNpc neurons. Two representative examples are shown of confocal images (63x objective) of single SNpc neurons immunostained for MPO (Dako, red) and αSyn (Syn505) (green) (Fig. 12A,C), with single channel αSyn (green) in panels B and D. MPO appeared to be localized to vesicles or granules while αSyn localized to a central deposit. Immunoperoxidase staining at lower magnification was performed (Fig. 12E) to quantitate the numbers of SNpc neurons that costain for MPO (black) and nitrated αSyn (red) as detected by monoclonal antibody nSyn14 which specifically detects nitrated αSyn [59]. Analysis of a minimum of three SNpc sections from eight PD brains and eight aged controls revealed that 30% of PD SNpc neurons costained for MPO and nSyn14 as compared to seven percent of aged control SNpc neurons (Fig. 12F). We conclude that expression of MPO in PD SNpc neurons is associated with increased levels of nitrated αSyn aggregates.

3.16 MPO colocalizes in neurons with MPO-specific HOCl-modified proteins in human PD brain

As MPO is the only enzyme able to generate HOCl by oxidizing Cl^-, staining for HOCl-modified proteins/epitopes is indicative of oxidative damage caused by the MPO-H_2O_2-Cl^- system [93]. To test for this oxidative damage in human PD SNpc, we used the specific monoclonal antibody (clone 2D10G9) raised against HOCl-modified proteins [60] that does not cross-react with other oxidative modifications such as that induced by 4-hydroxynonenal or malondialdehyde [61]. In melanized neurons, staining for HOCl-modified epitopes (black) was detected within neuromelanized vesicles (brown) (Fig. 12G). The arrows indicate three neurons in which the brown neuromelanin in vesicles is stained black by

2D10G9 immunostaining, in contrast to a nearby neuron with only brown neuromelanin. We examined PD SNpc sections from the eight PD cases and eight normal aged controls and counted the number of melanized neurons with HOCl-modified epitopes (Fig. 12H). Over 40% of the melanized neurons in the PD sections had HOCl-modified epitopes compared to 8% in the aged controls. We also observed the presence of MPO immunostaining (red) in melanized neurons that had been costained with 2D10G9 (black)(Fig. 12I). Lighter staining of 2D10G9 (Fig. 12J) allows better visualization of HOCl-modified epitope staining (black) within small vesicles in MPO positive (red) neurons. The percent of MPO positive neurons that contained HOCl-modified epitopes was more than 50% compared to 10% of the age matched control SNpc (Fig. 12K). These findings provide evidence that HOCl generated by the MPO-H_2O_2-Cl^- system oxidizes melanized neurons in human PD SNpc. As further evidence that MPO can be expressed in dopaminergic melanized neurons in PD SNpc, representative confocal images detected MPO (red) in SNpc neurons co-expressing tyrosine hydroxylase (green), a marker for dopaminergic neurons (Fig. 12L).

4. Discussion

This is the first study to demonstrate the atypical expression of hMPO in neurons in PD SNpc but not in neurons in normal aged brain. This result was complimented by finding the presence of aggregated αSyn in the MPO positive SNpc neurons as well as higher levels of nitrated αSyn and HOCl modified epitopes in MPO positive neurons. These findings provide evidence that MPO expression in PD SNpc neurons promotes oxidation and aggregation of αSyn, potentially contributing to neuropathology.

In addition to human PD brain, our study used mouse models of PD overexpressing the hαSyn A53T transgene along with hMPO to demonstrate the deleterious effects of MPO expression on motor capabilities. The hMPO-A53T model exhibited worse motor impairment and earlier onset of paralysis, along with increased nitrated αSyn, carbamylated αSyn, insoluble αSyn aggregates, MPO-generated HOCl epitopes, and nitroTyr. Importantly the hMPO transgene had no effect on motor capabilities in the absence of the A53T transgene. This indicates the deleterious impact of MPO requires the presence of hαSyn expression, suggesting that nitration, chlorination, and carbamylation of αSyn via the MPO-H_2O_2 system creates more neurotoxic forms. This is consistent with our earlier findings in a mutant amyloid precursor protein (APP23) overexpressing mouse model of AD [26] in that the hMPO transgene in the presence of APP23 expression led to greater phospholipid peroxidation in brain, while the hMPO transgene alone did not increase phospholipid peroxidation. This indicates that the pathogenic effects of MPO expression require the presence of αSyn or β-amyloid which can form pathological aggregates when oxidized/nitrated.

hMPO is considered a myeloid specific protein, present at high levels in circulating neutrophils and monocytes (5 or 1% of total cell protein content, respectively). However, recent findings by our group and others show that the MPO gene can be atypically/aberrantly expressed in some non-myeloid cells under stress conditions such as astrocytes and neurons in AD [25–27] and astrocytes in a 1-methyl-4-phenyl-1,2,3,6-tetrahydropyrine (MPTP) induced model of PD [22] as well as some cancer cells [47, 94]. In addition, we

previously found MPO expression in microglia in AD by immunohistochemistry, which was unexpected because MPO expression is thought to be limited to bone marrow myeloid precursors [25]. In epidemiological studies, the higher expressing −463G MPO polymorphism has been associated with increased risk or earlier onset of AD [25, 34–38] as well as risk for several types of cancer [39–46, 95] suggesting a causative or contributory role for MPO expression in non-myeloid cells in these disease states.

The normal function of MPO is to combat invading microbes. This raises the interesting possibility that inflammatory signals in PD/AD brain may induce low levels of hMPO expression in neurons or other non-myeloid cells to counteract a perceived microbial presence. Recent reports suggest that bacteria are able to enter the brain via a number of avenues including the nose, lung, gut and mouth and may influence the initiation and progression of neurodegenerative diseases [96]. As one recent example, postmortem analysis of AD brain showed 96% were immunopositive for the virulence factors known as gigipains from the bacteria that causes gingivitis, *Porphyromonas gingivalis* [97]. Together these findings suggest that the hMPO gene may be induced by stress in neurons, astrocytes, or microglia, and the cell type affected depends on the stressor such as αSyn or β-amyloid aggregates.

There have been no prior studies of hMPO effects in PD/synucleinopathies using transgenic αSyn expressing mouse models. An earlier study used the MPTP neurotoxin model of PD to show that intraperitoneal MPTP injection resulted in reduced numbers of tyrosine hydroxylase positive neurons, and increased MPO expression in astrocytes. In addition, the MPTP induced neuropathology was reduced in MPO-deficient mice [22]. In the present study, we show evidence of MPO involvement in PD using transgenic mice expressing hMPO and human A53T-αSyn. These studies show hMPO protein is expressed in subsets of neurons, leading to greater motor impairment associated with increased nitrated, crosslinked and insoluble forms of αSyn. Importantly, qPCR showed that the levels of hMPO mRNA are much higher than mMPO mRNA in hMPO-A53T brain. The hMPO transgene is present as a single copy, indicating that the higher levels of hMPO mRNA is reflective of higher activity of the hMPO promoter in the brain. Moreover, hMPO transgene expression was increased ~40% in the presence of the A53T transgene, suggesting αSyn neurotoxicity induces hMPO gene expression, perhaps through promoter elements responsive to stress. If so, this could lead to a vicious cycle of increased MPO expression causing more nitration of αSyn creating more neurotoxic dimers and aggregates.

Sources of H_2O_2 for MPO activity in the brain

MPO enzyme activity requires a source of H_2O_2. In the brain there are three likely sources. First, mitochondrial electron transport chain dysfunction generates superoxide which can be converted to H_2O_2 by superoxide dismutase [98, 99]. A second source is monoamine oxidases, which catalyze the deamination of dopamine which produces H_2O_2 as a by-product (reviewed [100]). A third is the nicotinamide adenine dinucleotide phosphate oxidases (NADPH) (reviewed [101]) some of which are expressed in the brain and increased in PD and models of PD (reviewed [102]. The two likely sources of H_2O_2 are the mitochondrial electron transport chain dysfunction given that αSyn has been shown to

promote mitochondrial dysfunction in PD models [99, 103] and/or the induced expression of NADPH oxidases [102]. NADPH oxidase is known to be induced in patients with PD [104]. Blocking the activity of NADPH oxidase attenuated the disease severity in an MPTP model [105] as well as in a paraquat model of PD [106]. Interestingly, hMPO transgenic mice in the absence of αSyn do not have motor dysfunction or other pathology. This suggests that in the absence of hαSyn, there is no significant production of H_2O_2 by the mechanisms just described eliminating MPO activity and neuropathology.

Oxidation of tyrosine by MPO leads to chlorotyrosine, nitroTyr and dityrosine crosslinking.

MPO is involved in several pathways that can lead to oxidation of tyrosines in αSyn. In the presence of halides (Cl^-, Br^-, I^-) and the pseudohalide SCN^-, MPO utilizes H_2O_2 to generate the corresponding hypohalous acids. Under physiological conditions, Cl^- is the preferred substrate and a potent chlorinating oxidant. The ability of MPO to react with Cl^- is unique and thus, oxidation products generated in this reaction are unique to MPO (reviewed [93, 107]) (see Fig. 2 and 11). In addition to the generation of chlorotyrosine, HOCl has been shown to oxidize dopamine to create neurotoxic forms [108, 109].

In the presence of H_2O_2, MPO can also oxidize the aromatic benzene ring of tyrosine resulting in the formation of a tyrosyl radical which can lead to the dimerization of tyrosines through formation of *o,o'*-dityrosine [110]. This pathway could account for the dimerization and aggregation of αSyn in the presence of MPO. Another pathway involves NO°, which reacts rapidly with $O_2^{\circ-}$ to form $ONOO^-$, a reactive nitrogen species [111]. Furthermore, the oxidation of NO produces nitrite that reacts with MPO and H_2O_2 to generate nitrogen dioxide radical (NO_2°). Both $ONOO^-$ and NO_2° generate 3-nitroTyr [21] and are likely to contribute to the nitration of αSyn seen in the MPO-A53T model [112, 113]. While there exist alternative mechanisms to generate 3-nitroTyr, our results show that the expression of the hMPO transgene in the A53T mouse brain increases the levels of 3-nitroTyr, indicating that some of this increase in 3-nitroTyr is due to MPO expression.

Deleterious versus protective effects of carbamylation of αSyn by MPO.

MPO also catalyzes the reaction of H_2O_2 and SCN^- to form hypothiocyanous acid (HOSCN) [82]. HOSCN plays a beneficial role as a bacteriostatic agent but may also have deleterious effects on normal cellular function [114]. MPO-catalyzed oxidation of SCN^- has been linked to carbamylation of lipoproteins of the low- (LDL, [115]) and high-density range (HDL, [116]), leading to pro-atherosclerotic events including cholesterol accumulation and foam-cell formation. This is particularly evident in postmortem studies of smokers in which higher levels of SCN^- were observed and correlated with atherogenic biomarkers such as oxidized LDL, apolipoprotein E deposition, and presence of macrophage foam cells [115]. Similarly, in the case of HDL carbamylation, one carbamylysine residue per HDL-associated apolipoprotein A-1 was sufficient to induce cholesterol accumulation and lipid droplet formation in macrophages [116]. Sources of SCN^- include tobacco smoke, environmental pollutants, diet, or the metabolism of cyanide by sulfurtransferases [117]. Recently, an alternative source of cyanate was described [118]. MPO was found to catalyze the two-electron oxidation of cyanide to cyanate and promote the carbamylation of taurine, lysine and LDL [118]. SCN^- may have beneficial effects due to the fact that HOSCN is less

toxic than HOCl [119, 120]. HOSCN is a less powerful oxidizing agent and more thiol-specific compared to HOCl and HOBr [121, 122]. This may partly explain our finding that fewer multimers of αSyn were generated via MPO and SCN^- treatment than with MPO and nitrite treatment (Fig. 8).

Several animal studies suggest that SCN^- treatment may be useful therapeutically. Nebulized SCN^- effectively reduced bacterial load, infection mediated morbidity, and airway inflammation in mice infected with P. *aeruginosa* [123]. In another example, supplementation of SCN^- in the drinking water has been tested as a possible therapy to reduce the oxidative damage by the MPO product HOCl. When humanized MPO mice were crossed to $LDL^{-/-}$ mice and treated with or without SCN^- in the drinking water, there was a 2-fold increase in plasma SCN^- and a 26% reduction in plaque area in the SCN^- treated mice compared to control mice [124]. Further studies are warranted to evaluate the anti-inflammatory effects of SCN^- in chronic neurodegenerative diseases involving MPO such as PD, in that SCN^- may counter the negative impact of MPO/HOCl and MPO/nitration.

Monomeric MPO is trafficked to secretory vesicles and could thus propagate αSyn pathology

In myeloid cells, MPO is expressed as a 90 kDa monomer termed proMPO which is proteolytically processed to heavy (59 kDa) and light (15 kDa) chains that are linked by disulfides and complexed with heme to generate the mature tetramer that is localized to storage vesicles [72]. Interestingly, the highly related lactoperoxidase (LPO) is produced as a monomer and secreted into breast milk as a microbicidal agent [125–127]. The MPO and LPO genes exist as a tandem repeat inverted tail to tail [128], suggesting that MPO and LPO could share genetic elements that lead to the generation of the secreted monomer in non-myeloid cells. As shown here, MPO is produced as the monomer in hMPO-A53T brain, suggesting that neurons lack the processing and trafficking machinery for MPO that is present in neutrophil precursors. This raises the possibility that monomer MPO could be secreted from neurons, potentially leading to oxidative damage to neighboring neurons in PD or secreted in vesicles along with αSyn [129]. We and others have shown that cells transfected with MPO cDNA can express the proMPO protein and secrete enzymatically active proMPO into the media [56, 130–132]. ProMPO is present in human serum and is active [56, 133, 134]. The source of proMPO in serum remains an unresolved question as mature neutrophils do not contain proMPO. One likely source of proMPO in serum is bone marrow myeloid precursors where MPO is synthesized as the monomer and then processed and packaged into azurophilic granules/vesicles in neutrophils. In support of this hypothesis, the neutrophil precursor cell line HL-60 has been shown to secrete proMPO [135, 136]. The findings here, however, raise the interesting possibility that under some conditions (e.g. cell stress) MPO expression can be induced in non-myeloid cell types primarily as the precursor secreted form. Furthermore, the release of proMPO with αSyn in secretory vesicles may provide a means to disseminate neurotoxic αSyn and propagate disease, possibly through the release of exosomes [129].

Regulation of MPO gene expression in non-myeloid cells

MPO expression and processing in myeloid cells has been well studied [30, 31, 137–139]. The evidence for MPO expression in non-myeloid cells is limited but gaining in acceptance [140]. Most evidence comes from the analysis of epithelial cell derived cancers. MPO has been detected by immunohistochemistry in ovarian cancer epithelial cells [47, 94] and prostate epithelial cells [141]. Recently, MPO mRNA and protein was detected in primary endothelial cells and in a number of endothelial cell lines [142]. In AD, MPO has been detected in astrocytes [26], microglia [25], and neurons [27]. MPO has been previously detected in astrocytes in PD [22], and in this study in neurons by immunohistochemistry (Fig. 1) and MPO mRNA by RNAscope *in situ* hybridization (Fig. 3). The mechanisms which induce hMPO expression in non-myeloid cells are not defined.

The hMPO gene is regulated in part through an upstream Alu element with several overlapping hexamer halfsites related to the consensus 5'-AGGTCA-3' that are recognized by members of the nuclear receptor superfamily of transcription factors including PPARa/Y, estrogen hormone receptor, thyroid hormone receptor, as well as SP1 [30–32]. There are over one million Alu elements dispersed throughout the human genome. Alu elements are primate specific retroposons that evolved to contain these receptor binding sites over a period of ~40 million years [31, 33]. The first hexamer half-site in the MPO Alu includes the −463G/A polymorphism with the G at this position being associated with higher expression levels and creating an SP1 binding site [29, 31]. The −463G allele is associated with increased risk for AD, atherosclerosis, cardiovascular disease, lung cancer, leukemia, and breast cancer in epidemiological studies by our lab and others [25, 34–38, 143, 144]. Findings here raise the possibility that neurotoxic forms of αSyn could lead to signals similar to those elicited by microbial infection, acting on MPO promoter elements, possibly those in the Alu sites, that trigger MPO gene expression in neurons, and the consequence is greater nitration and oxidation of αSyn leading to neuron loss. The low level of MPO expression induced in neurons or astrocytes presumably was protective in primate evolution, providing a line of defense against microbes in brain trauma, but in the present day with longer human lifespans, MPO is erroneously induced by αSyn or β-amyloid aggregates promoting or even initiating PD or AD, respectively.

Accumulation of αSyn aggregates at the terminus of CA2 dendrites expressing ATF4.

A number of studies provide evidence for the existence of ER stress and the UPR in PD (reviewed [145]). UPR mediators PERK and phospho-eukaryotic translation initiation factor 2A (p-eIF2a have been detected in post mortem PD brain colocalizing with αSyn deposits [146]. In various αSyn transgenic mouse models, there is evidence of induction of UPR mediators including BiP, XBP1, CHOP, and ATF4 [147–150]. In the present study, we detected ATF4 in CA2 apical dendrites extending to an accumulation of αSyn aggregates localized at the terminus of CA2 apical dendrites in the stratum lacunosum moleculare (SLM) which receives synaptic input from axons projecting from the entorhinal cortex layer II (EC II) [90, 91]. This suggests the nitrated αSyn in the SLM may be in presynaptic terminals of EC II axons in contact with CA2 dendrites. UPR mediator CHOP and cleaved caspase-3 were detected in the hippocampal CA2 pyramidal layer which had a high proportion of dystrophic pyknotic nuclei suggestive of apoptosis. These findings raise the

possibility that contact of CA2 dendrites with nitrated αSyn aggregates in EC II axon terminals elicits stress leading to the apoptotic arm of the UPR. In a related finding, a prior study found that local application of β-amyloid 1–42 to rat embryonic hippocampal neurons induced ATF4 mRNA and protein expression in axons that led in retrograde fashion to CHOP-dependent neuron death involving p-eIF2a and cleaved caspase 3, indicating ER stress mediated apoptosis [151].

In addition to motor impairment, PD and DLB can be associated with social isolation and cognitive dysfunction [152–154]. Studies with human subjects and mouse models implicate hippocampal CA2 region with social recognition memory [86], temporal order memory, and cognitive impairment [87–89]. In another study, a correlation was found between the frequency of cortical Lewy bodies and the severity of neuritic degeneration in human CA2 [155]. Increased αSyn expression in hippocampus CA2/CA3 soma has also been reported for a mouse model of PD expressing mutant αSyn [156]. A study of postmortem PD/DLB brain showed highest accumulation of αSyn pathology in the CA2 region (Lewy neurites) and entorhinal cortex (EC) (Lewy bodies), correlating with degree of cognitive loss and neural atrophy [157]. That study showed that while CA2 had the highest level of αSyn pathology, memory impairment correlated more with CA1 which is thought to be downstream of CA2/EC pathology, suggesting that hippocampal αSyn pathology propagates beyond the initial site in CA2/EC to cause memory dysfunction in CA1 [157]. αSyn pathology could thus spread along interconnected hippocampal circuits. One possibility, based on our findings, is that the secretory form of MPO released from CA2 neurons in contact with CA1 and CA3 neurons could spread oxidative damage through these hippocampal regions.

Conclusions

Our findings show that MPO can be expressed in neurons in PD and in the humanized MPO-A53T mouse model of PD. In the model, MPO colocalizes in neurons with nitrated αSyn, carbamylated αSyn and HOCl-modified αSyn, correlating with greater αSyn aggregates and greater motor impairments on rotarod, balance beam, and wire hang. MPO is expressed as the precursor proMPO form that is secreted potentially spreading oxidative damage to neighboring neurons. These findings suggest that MPO may be a good target for the development of therapeutics to block its activity. This could lead to reduced αSyn oxidation and aggregation thus reducing PD severity. Several studies have hinted that MPO inhibitors can have a beneficial effect for the treatment of neurodegenerative diseases in humans. A phase I study using an MPO inhibitor to treat PD was recently completed [158]. Studies in animal models of Multiple Sclerosis (EAE) [159] and multiple system atrophy (MSA) [160, 161] indicate that blocking MPO activity lessens disease, pointing to the usefulness of developing MPO inhibitors. A safe and therapeutically effective blocker of MPO may be beneficial in other diseases where there is abnormal stress inducing MPO expression and causing oxidative damage. Side effects from blockage of MPO are not to be expected, since MPO deficient individuals are mostly asymptomatic.

Acknowledgements

We would like to thank Richard Laura for helpful discussions. We would also like to thank Timothy Huang and Huaxi Xu for helpful advice on culturing primary neurons. We would like to thank Ana Arriola, Jacob Buck, James Chang, Kimberley Pham, Kurt Sakurada, Eitan Shemuelian, Eric Tong, and Maggie Yamin for technical assistance. We would also like to thank Guillermina Garcia in the Histology facility for her assistance, and Leslie Boyd in the Cell Imaging facility at Sanford Burnham Prebys Medical Discovery Institute (La Jolla CA) for helping us with the confocal microscopy.

Funding: This work was supported in part by the NIH (ROI NS074303, ROI AG017879, and ROI AG040623 to WFR. Additional funding to support these studies has been generously provided by Sanford Burnham Prebys Medical Discovery Institute (La Jolla CA) and the Austrian National Bank (17600).

Abbreviations:

αSyn	α-Synuclein
MPO	Myeloperoxidase
hMPO	human myeloperoxidase
mMPO	mouse myeloperoxidase
hMPO tg	human myeloperoxidase transgenic
NO	nitric oxide
HOCl	hypochlorous acid
ER	endoplasmic reticulum
UPR	unfolded protein response
ATF4	activating transcription factor 4
CHOP	C/EBP homologous protein
BiP	binding immunoglobulin protein
XBP1	X box binding protein 1
PD	Parkinson’s disease
AD	Alzheimer’s disease
DLB	dementia with Lewy Bodies
SNpc	substantia nigra pars compacta
SN	substantia nigra
SLM	stratum lacunosum moleculare
ICII	entorhinal cortex II
APP	amyloid precursor protein
APP23	mutant amyloid precursor protein

A53T	αSyn gene with the A53T mutation
MAP2	microtubule-associated protein
nitroTyr	nitrated tyrosine
MPTP	1-methyl-4-phenyl-1,2,3,6-tetrahydropyrine
NADPH	nicotinamide adenine dinucleotide phosphate
SCN	thiocyanate
HOSCN	hypothiocyanous acid
LDL	low density lipoproteins
HDL	high density lipoproteins
MS	multiple sclerosis
MSA	multiple system atrophy
MF	mossy fiber tract
MBP	myelin basic protein
qPCR	quantitative polymerase chain reaction
DNAse I	deoxyribonuclease I
PFA	paraformaldehyde
ELISA	enzyme linked immunosorbent assay

References

1. Goetz CG, McGhiey A. The movement disorder society and movement disorders: a modern history. Mov Disord. 2011;26(6):939–46. doi: 10.1002/mds.23689. [PubMed: 21626540]
2. Poewe W, Seppi K, Tanner CM, Halliday GM, Brundin P, Volkmann J, et al. Parkinson disease. Nat Rev Dis Primers. 2017;3:17013. doi: 10.1038/nrdp.2017.13. [PubMed: 28332488]
3. Spillantini MG, Schmidt ML, Lee VM, Trojanowski JQ, Jakes R, Goedert M. Alpha-synuclein in Lewy bodies. Nature. 1997;388(6645):839–40. doi: 10.1038/42166. [PubMed: 9278044]
4. Rosborough K, Patel N, Kalia LV. alpha-Synuclein and Parkinsonism: Updates and Future Perspectives. Curr Neurol Neurosci Rep. 2017;17(4):31. doi: 10.1007/s11910-017-0737-y. [PubMed: 28324300]
5. Konno T, Ross OA, Puschmann A, Dickson DW, Wszolek ZK. Autosomal dominant Parkinson's disease caused by SNCA duplications. Parkinsonism Relat Disord. 2016;22 Suppl 1:S1–6. doi: 10.1016/j.parkreldis.2015.09.007. [PubMed: 26350119]
6. Hashimoto M, Hsu LJ, Sisk A, Xia Y, Takeda A, Sundsmo M, et al. Human recombinant NACP/alpha-synuclein is aggregated and fibrillated in vitro: relevance for Lewy body disease. Brain Res. 1998;799(2):301–6. [PubMed: 9675319]
7. Perry TL, Yong VW. Idiopathic Parkinson's disease, progressive supranuclear palsy and glutathione metabolism in the substantia nigra of patients. Neurosci Lett. 1986;67(3):269–74. [PubMed: 3737015]

8. Jenner P, Dexter DT, Sian J, Schapira AH, Marsden CD. Oxidative stress as a cause of nigral cell death in Parkinson's disease and incidental Lewy body disease. The Royal Kings and Queens Parkinson's Disease Research Group. Ann Neurol. 1992;32 Suppl:S82–7. [PubMed: 1510385]
9. Yoritaka A, Hattori N, Uchida K, Tanaka M, Stadtman ER, Mizuno Y. Immunohistochemical detection of 4-hydroxynonenal protein adducts in Parkinson disease. Proc Natl Acad Sci U S A. 1996;93(7):2696–701. [PubMed: 8610103]
10. Duda JE, Giasson BI, Chen Q, Gur TL, Hurtig HI, Stern MB, et al. Widespread nitration of pathological inclusions in neurodegenerative synucleinopathies. Am J Pathol. 2000;157(5):1439–45. [PubMed: 11073803]
11. Nunomura A, Moreira PI, Lee HG, Zhu X, Castellani RJ, Smith MA, et al. Neuronal death and survival under oxidative stress in Alzheimer and Parkinson diseases. CNS Neurol Disord Drug Targets. 2007;6(6):411–23. [PubMed: 18220780]
12. Dexter DT, Carter CJ, Wells FR, Javoy-Agid F, Agid Y, Lees A, et al. Basal lipid peroxidation in substantia nigra is increased in Parkinson's disease. J Neurochem. 1989;52(2):381–9. [PubMed: 2911023]
13. Alam ZI, Daniel SE, Lees AJ, Marsden DC, Jenner P, Halliwell B. A generalised increase in protein carbonyls in the brain in Parkinson's but not incidental Lewy body disease. J Neurochem. 1997;69(3):1326–9. [PubMed: 9282961]
14. Alam ZI, Jenner A, Daniel SE, Lees AJ, Cairns N, Marsden CD, et al. Oxidative DNA damage in the parkinsonian brain: an apparent selective increase in 8-hydroxyguanine levels in substantia nigra. J Neurochem. 1997;69(3):1196–203. [PubMed: 9282943]
15. Chavarria C, Souza JM. Oxidation and nitration of alpha-synuclein and their implications in neurodegenerative diseases. Arch Biochem Biophys. 2013;533(1–2):25–32. doi: 10.1016/j.abb.2013.02.009. [PubMed: 23454347]
16. He YX, Yu ZW, Chen SD. Alpha-synuclein nitration and its implications in Parkinson's disease. ACS Chem Neurosci. 2018. doi: 10.1021/acschemneuro.8b00288.
17. Kurz A, Double KL, Lastres-Becker T, Tozzi A, Tantucci M, Bockhart V, et al. A53T-alpha-synuclein overexpression impairs dopamine signaling and striatal synaptic plasticity in old mice. PLoS One. 2010;5(7):e11464. doi: 10.1371/journal.pone.0011464. [PubMed: 20628651]
18. Scott DA, Tabarean T, Tang Y, Cartier A, Masliah E, Roy S. A pathologic cascade leading to synaptic dysfunction in alpha-synuclein-induced neurodegeneration. J Neurosci. 2010;30(24):8083–95. doi: 10.1523/JNEUR0SCT.1091-10.2010. [PubMed: 20554859]
19. Xu J, Wu XS, Sheng J, Zhang Z, Yue HY, Sun L, et al. alpha-Synuclein Mutation Inhibits Endocytosis at Mammalian Central Nerve Terminals. J Neurosci. 2016;36(16):4408–14. doi: 10.1523/JNEUR0SCT.3627-15.2016. [PubMed: 27098685]
20. Dias V, Junn E, Mouradian MM. The role of oxidative stress in Parkinson's disease. J Parkinsons Dis. 2013;3(4):461–91. doi: 10.3233/JPD-130230. [PubMed: 24252804]
21. Malle E, Buch T, Grone HJ. Myeloperoxidase in kidney disease. Kidney Tnt. 2003;64(6):1956–67. doi: 10.1046/j.1523-1755.2003.00336.x.
22. Choi DK, Pennathur S, Perier C, Tieu K, Teismann P, Wu DC, et al. Ablation of the inflammatory enzyme myeloperoxidase mitigates features of Parkinson's disease in mice. J Neurosci. 2005;25(28):6594–600. doi: 10.1523/JNEUR0SCT.0970-05.2005. [PubMed: 16014720]
23. Klebanoff SJ, Kettle AJ, Rosen H, Winterbourn CC, Nauseef WM. Myeloperoxidase: a front-line defender against phagocytosed microorganisms. J Leukoc Biol. 2013;93(2):185–98. doi: 10.1189/jlb.0712349. [PubMed: 23066164]
24. Winterbourn CC, Kettle AJ, Hampton MB. Reactive Oxygen Species and Neutrophil Function. Annu Rev Biochem. 2016;85:765–92. 10.1146/annurev-biochem-060815-014442. [PubMed: 27050287]
25. Reynolds WF, Rhees J, Maciejewski D, Paladino T, Sieburg H, Maki RA, et al. Myeloperoxidase polymorphism is associated with gender specific risk for Alzheimer's disease. Exp Neurol. 1999;155(1):31–41. doi: 10.1006/exnr.1998.6977. [PubMed: 9918702]
26. Maki RA, Tyurin VA, Lyon RC, Hamilton RL, DeKosky ST, Kagan VE, et al. Aberrant expression of myeloperoxidase in astrocytes promotes phospholipid oxidation and memory deficits in a

mouse model of Alzheimer disease. J Biol Chem. 2009;284(5):3158–69. doi: 10.1074/jbc.M807731200. [PubMed: 19059911]

27. Green PS, Mendez AJ, Jacob JS, Crowley JR, Growdon W, Hyman BT, et al. Neuronal expression of myeloperoxidase is increased in Alzheimer's disease. J Neurochem. 2004;90(3):724–33. doi: 10.1111/j.1471-4159.2004.02527.x. [PubMed: 15255951]
28. Gellhaar S, Sunnemark D, Eriksson H, Olson L, Galter D. Myeloperoxidase-immunoreactive cells are significantly increased in brain areas affected by neurodegeneration in Parkinson's and Alzheimer's disease. Cell Tissue Res. 2017;369(3):445–54. doi: 10.1007/s00441-017-2626-8. [PubMed: 28466093]
29. Castellani LW, Chang JJ, Wang X, Lusis AJ, Reynolds WF. Transgenic mice express human MPO -463G/A alleles at atherosclerotic lesions, developing hyperlipidemia and obesity in −463G males. J Lipid Res. 2006;47(7):1366–77. doi: 10.1194/jlr.M600005-JLR200. [PubMed: 16639078]
30. Kumar AP, Piedrafita FJ, Reynolds WF. Peroxisome proliferator-activated receptor gamma ligands regulate myeloperoxidase expression in macrophages by an estrogen-dependent mechanism involving the - 463GA promoter polymorphism. J Biol Chem. 2004;279(9):8300–15. doi: 10.1074/jbc.M311625200. [PubMed: 14668325]
31. Piedrafita FJ, Molander RB, Vansant G, Orlova EA, Pfahl M, Reynolds WF. An Alu element in the myeloperoxidase promoter contains a composite SP1-thyroid hormone-retinoic acid response element. J Biol Chem. 1996;271(24):14412–20. [PubMed: 8662930]
32. Reynolds WF, Kumar AP, Piedrafita FJ. The human myeloperoxidase gene is regulated by LXR and PPARalpha ligands. Biochem Biophys Res Commun. 2006;349(2):846–54. doi: 10.1016/j.bbrc.2006.08.119. [PubMed: 16956579]
33. Vansant G, Reynolds WF. The consensus sequence of a major Alu subfamily contains a functional retinoic acid response element. Proc Natl Acad Sci U S A. 1995;92(18):8229–33. [PubMed: 7667273]
34. Reynolds WF, Hiltunen M, Pirskanen M, Mannermaa A, Helisalmi S, Lehtovirta M, et al. MPO and APOEepsilon4 polymorphisms interact to increase risk for AD in Finnish males. Neurology. 2000;55(9):1284–90. [PubMed: 11087769]
35. Crawford FC, Freeman MJ, Schinka JA, Morris MD, Abdullah LI, Richards D, et al. Association between Alzheimer's disease and a functional polymorphism in the Myeloperoxidase gene. Exp Neurol. 2001;167(2):456–9. doi: 10.1006/exnr.2000.7560. [PubMed: 11161635]
36. Leininger-Muller B, Hoy A, Herbeth B, Pfister M, Serot JM, Stavljenic-Rukavina M, et al. Myeloperoxidase G-463A polymorphism and Alzheimer's disease in the ApoEurope study. Neurosci Lett. 2003;349(2):95–8. [PubMed: 12946561]
37. Zappia M, Manna I, Serra P, Cittadella R, Andreoli V, La Russa A, et al. Increased risk for Alzheimer disease with the interaction of MPO and A2M polymorphisms. Arch Neurol. 2004;61(3):341–4. doi: 10.1001/archneur.61.3.341. [PubMed: 15023809]
38. Pope SK, Kritchevsky SB, Ambrosone C, Yaffe K, Tylavsky F, Simonsick EM, et al. Myeloperoxidase polymorphism and cognitive decline in older adults in the Health, Aging, and Body Composition Study. Am J Epidemiol. 2006;163(12):1084–90. doi: 10.1093/aje/kwj146. [PubMed: 16641309]
39. Hoy A, Tregouet D, Leininger-Muller B, Poirier O, Maurice M, Sass C, et al. Serum myeloperoxidase concentration in a healthy population: biological variations, familial resemblance and new genetic polymorphisms. Eur J Hum Genet. 2001;9(10):780–6. doi: 10.1038/sj.ejhg.5200702. [PubMed: 11781690]
40. Pecoits-Filho R, Stenvinkel P, Marchlewska A, Heimburger O, Barany P, Hoff CM, et al. A functional variant of the myeloperoxidase gene is associated with cardiovascular disease in end-stage renal disease patients. Kidney Int Suppl. 2003;(84):S172–6. doi: 10.1046/j.1523-1755.63.s84.32.x. [PubMed: 12694338]
41. Makela R, Karhunen PJ, Kunnas TA, Ilveskoski E, Kajander OA, Mikkelsson J, et al. Myeloperoxidase gene variation as a determinant of atherosclerosis progression in the abdominal and thoracic aorta: an autopsy study. Lab Invest. 2003;83(7):919–25. [PubMed: 12861032]

42. Makela R, Laaksonen R, Janatuinen T, Vesalainen R, Nuutila P, Jaakkola O, et al. Myeloperoxidase gene variation and coronary flow reserve in young healthy men. J Biomed Sci. 2004;11(1):59–64. doi: 10.1159/000075289. [PubMed: 14730210]
43. Asselbergs FW, Reynolds WF, Cohen-Tervaert JW, Jessurun GA, Tio RA. Myeloperoxidase polymorphism related to cardiovascular events in coronary artery disease. Am J Med. 2004;116(6): 429–30. doi: 10.1016/j.amjmed.2003.10.025. [PubMed: 15006595]
44. Rudolph V, Rudolph TK, Kubala L, Clauberg N, Maas R, Pekarova M, et al. A myeloperoxidase promoter polymorphism is independently associated with mortality in patients with impaired left ventricular function. Free Radic Biol Med. 2009;47(11):1584–90. doi: 10.1016/j.freeradbiomed. 2009.09.001. [PubMed: 19735726]
45. Schabath MB, Spitz MR, Hong WK, Delclos GL, Reynolds WF, Gunn GB, et al. A myeloperoxidase polymorphism associated with reduced risk of lung cancer. Lung Cancer. 2002;37(1):35–40. [PubMed: 12057865]
46. Yang JP, Wang WB, Yang XX, Yang L, Ren L, Zhou FX, et al. The MPO-463G>A polymorphism and lung cancer risk: a meta-analysis based on 22 case-control studies. PLoS One. 2013;8(6):e65778. doi: 10.1371/journal.pone.0065778. [PubMed: 23840365]
47. Castillo-Tong DC, Pils D, Heinze G, Braicu I, Sehouli J, Reinthaller A, et al. Association of myeloperoxidase with ovarian cancer. Tumour Biol. 2014;35(1): 141–8. doi: 10.1007/ s13277-013-1017-3. [PubMed: 23893381]
48. Kumar AP, Ryan C, Cordy V, Reynolds WF. Inducible nitric oxide synthase expression is inhibited by myeloperoxidase. Nitric Oxide. 2005;13(1):42–53. doi: 10.1016/j.niox.2005.04.002. [PubMed: 15893945]
49. Chandra S, Gallardo G, Fernandez-Chacon R, Schluter OM, Sudhof TC. Alpha-synuclein cooperates with CSPalpha in preventing neurodegeneration. Cell. 2005;123(3):383–96. doi: 10.1016/j.cell.2005.09.028. [PubMed: 16269331]
50. Martin LJ, Semenkow S, Hanaford A, Wong M. Mitochondrial permeability transition pore regulates Parkinson's disease development in mutant alpha-synuclein transgenic mice. Neurobiol Aging. 2014;35(5):1132–52. doi: 10.1016/j.neurobiolaging.2013.11.008. [PubMed: 24325796]
51. Rothman SM, Griffioen KJ, Vranis N, Ladenheim B, Cong WN, Cadet JL, et al. Neuronal expression of familial Parkinson's disease A53T alpha-synuclein causes early motor impairment, reduced anxiety and potential sleep disturbances in mice. J Parkinsons Dis. 2013;3(2):215–29. doi: 10.3233/JPD-120130. [PubMed: 23938351]
52. Rockenstein E, Mallory M, Hashimoto M, Song D, Shults CW, Lang I, et al. Differential neuropathological alterations in transgenic mice expressing alpha-synuclein from the platelet-derived growth factor and Thy-1 promoters. J Neurosci Res. 2002;68(5):568–78. doi: 10.1002/jnr. 10231. [PubMed: 12111846]
53. Fleming SM, Salcedo J, Fernagut PO, Rockenstein E, Masliah E, Levine MS, et al. Early and progressive sensorimotor anomalies in mice overexpressing wild-type human alpha-synuclein. J Neurosci. 2004;24(42):9434–40. doi: 10.1523/JNEUROSCI.3080-04.2004. [PubMed: 15496679]
54. Masliah E, Rockenstein E, Veinbergs I, Mallory M, Hashimoto M, Takeda A, et al. Dopaminergic loss and inclusion body formation in alpha-synuclein mice: implications for neurodegenerative disorders. Science. 2000;287(5456):1265–9. [PubMed: 10678833]
55. Shults CW, Rockenstein E, Crews L, Adame A, Mante M, Larrea G, et al. Neurological and neurodegenerative alterations in a transgenic mouse model expressing human alpha-synuclein under oligodendrocyte promoter: implications for multiple system atrophy. J Neurosci. 2005;25(46):10689–99. doi: 10.1523/JNEUROSCI.3527-05.2005. [PubMed: 16291942]
56. Laura RP, Dong D, Reynolds WF, Maki RA. T47D Cells Expressing Myeloperoxidase Are Able to Process, Traffic and Store the Mature Protein in Lysosomes: Studies in T47D Cells Reveal a Role for Cys319 in MPO Biosynthesis that Precedes Its Known Role in Inter-Molecular Disulfide Bond Formation. PLoS One. 2016;11(2):e0149391. doi: 10.1371/journal.pone.0149391. [PubMed: 26890638]
57. Duda JE, Giasson BI, Mabon ME, Lee VM, Trojanowski JQ. Novel antibodies to synuclein show abundant striatal pathology in Lewy body diseases. Ann Neurol. 2002;52(2):205–10. doi: 10.1002/ ana.10279. [PubMed: 12210791]

58. Baba M, Nakajo S, Tu PH, Tomita T, Nakaya K, Lee VM, et al. Aggregation of alpha-synuclein in Lewy bodies of sporadic Parkinson's disease and dementia with Lewy bodies. Am J Pathol. 1998;152(4):879–84. [PubMed: 9546347]
59. Giasson BI, Duda JE, Murray IV, Chen Q, Souza JM, Hurtig HI, et al. Oxidative damage linked to neurodegeneration by selective alpha-synuclein nitration in synucleinopathy lesions. Science. 2000;290(5493):985–9. [PubMed: 11062131]
60. Malle E, Woenckhaus C, Waeg G, Esterbauer H, Grone EF, Grone HJ. Immunological evidence for hypochlorite-modified proteins in human kidney. Am J Pathol. 1997;150(2):603–15. [PubMed: 9033274]
61. Malle E, Hazell L, Stocker R, Sattler W, Esterbauer H, Waeg G. Immunologic detection and measurement of hypochlorite-modified LDL with specific monoclonal antibodies. Arterioscler Thromb Vasc Biol. 1995;15(7):982–9. [PubMed: 7541296]
62. Vanichkitrungruang S, Chuang CY, Hawkins CL, Hammer A, Hoefler G, Malle E, et al. Oxidation of human plasma fibronectin by inflammatory oxidants perturbs endothelial cell function. Free Radic Biol Med. 2019;136:118–34. 10.1016/j.freeradbiomed.2019.04.003. [PubMed: 30959171]
63. Games D, Seubert P, Rockenstein E, Patrick C, Trejo M, Ubhi K, et al. Axonopathy in an alpha-synuclein transgenic model of Lewy body disease is associated with extensive accumulation of C-terminal-truncated alpha-synuclein. Am J Pathol. 2013;182(3):940–53. doi: 10.1016/j.ajpath.2012.11.018. [PubMed: 23313024]
64. Hansen LA. The Lewy body variant of Alzheimer disease. J Neural Transm Suppl. 1997;51:83–93. [PubMed: 9470130]
65. Whittaker VP, Michaelson IA, Kirkland RJ. The separation of synaptic vesicles from nerve-ending particles ('synaptosomes'). Biochem J. 1964;90(2):293–303. [PubMed: 5834239]
66. Brill LM, Motamedchaboki K, Wu S, W olf DA. Comprehensive proteomic analysis of Schizosaccharomyces pombe by two-dimensional HPLC-tandem mass spectrometry. Methods. 2009;48(3):311–9. doi: 10.1016/j.ymeth.2009.02.023. [PubMed: 19272449]
67. Holzer M, Zangger K, El-Gamal D, Binder V, Curcic S, Konya V, et al. Myeloperoxidase-derived chlorinating species induce protein carbamylation through decomposition of thiocyanate and urea: novel pathways generating dysfunctional high-density lipoprotein. Antioxid Redox Signal. 2012;17(8):1043–52. doi: 10.1089/ars.2011.4403. [PubMed: 22462773]
68. Damm M, Holzer M, Radspieler G, Marsche G, Kappe CO. Microwave-assisted high-throughput acid hydrolysis in silicon carbide microtiter platforms--a rapid and low volume sample preparation technique for total amino acid analysis in proteins and peptides. J Chromatogr A. 2010;1217(50):7826–32. doi: 10.1016/j.chroma.2010.10.062. [PubMed: 21056423]
69. Livak KJ, Schmittgen TD. Analysis of relative gene expression data using real-time quantitative PCR and the 2(-Delta Delta C(T)) Method. Methods. 2001;25(4):402–8. doi: 10.1006/meth.2001.1262. [PubMed: 11846609]
70. Huang TY, Zhao Y, Li X, Wang X, Tseng IC, Thompson R, et al. SNX27 and SORLA Interact to Reduce Amyloidogenic Subcellular Distribution and Processing of Amyloid Precursor Protein. J Neurosci. 2016;36(30):7996–8011. doi: 10.1523/JNEUROSCI.0206-16.2016. [PubMed: 27466343]
71. Huang TY, Zhao Y, Jiang LL, Li X, Liu Y, Sun Y, et al. SORLA attenuates EphA4 signaling and amyloid beta-induced neurodegeneration. J Exp Med. 2017;214(12):3669–85. doi: 10.1084/jem.20171413. [PubMed: 29114064]
72. Nauseef WM. Biosynthesis of human myeloperoxidase. Arch Biochem Biophys. 2018;642:1–9. doi: 10.1016/j.abb.2018.02.001. [PubMed: 29408362]
73. Furtmuller PG, Jantschko W, Regelsberger G, Jakopitsch C, Moguilevsky N, Obinger C. A transient kinetic study on the reactivity of recombinant unprocessed monomeric myeloperoxidase. FEBS Lett. 2001;503(2–3):147–50. [PubMed: 11513872]
74. Wang F, Flanagan J, Su N, Wang LC, Bui S, Nielson A, et al. RNAscope: a novel in situ RNA analysis platform for formalin-fixed, paraffin-embedded tissues. J Mol Diagn. 2012;14(1):22–9. doi: 10.1016/j.jmoldx.2011.08.002. [PubMed: 22166544]

75. Waxman EA, Duda JE, Giasson BI. Characterization of antibodies that selectively detect alpha-synuclein in pathological inclusions. Acta Neuropathol. 2008;116(1):37–46. doi: 10.1007/s00401-008-0375-1. [PubMed: 18414880]
76. Vicente Miranda H, Cassio R, Correia-Guedes L, Gomes MA, Chegao A, Miranda E, et al. Posttranslational modifications of blood-derived alpha-synuclein as biochemical markers for Parkinson's disease. Sci Rep. 2017;7(1):13713. doi: 10.1038/s41598-017-14175-5. [PubMed: 29057912]
77. Hodara R, Norris EH, Giasson BI, Mishizen-Eberz AJ, Lynch DR, Lee VM, et al. Functional consequences of alpha-synuclein tyrosine nitration: diminished binding to lipid vesicles and increased fibril formation. J Biol Chem. 2004;279(46):47746–53. doi: 10.1074/jbc.M408906200. [PubMed: 15364911]
78. Schildknecht S, Gerding HR, Karreman C, Drescher M, Lashuel HA, Outeiro TF, et al. Oxidative and nitrative alpha-synuclein modifications and proteostatic stress: implications for disease mechanisms and interventions in synucleinopathies. J Neurochem. 2013;125(4):491–511. doi: 10.1111/jnc.12226. [PubMed: 23452040]
79. Medeiros AT, Soll LG, Tessari I, Bubacco L, Morgan JR. alpha-Synuclein Dimers Impair Vesicle Fission during Clathrin-Mediated Synaptic Vesicle Recycling. Front Cell Neurosci. 2017;11:388. doi: 10.3389/fncel.2017.00388. [PubMed: 29321725]
80. Souza JM, Giasson BI, Chen Q, Lee VM, Ischiropoulos H. Dityrosine cross-linking promotes formation of stable alpha-synuclein polymers. Implication of nitrative and oxidative stress in the pathogenesis of neurodegenerative synucleinopathies. J Biol Chem. 2000;275(24):18344–9. doi: 10.1074/jbc.M000206200. [PubMed: 10747881]
81. Pattison DI, Davies MJ, Hawkins CL. Reactions and reactivity of myeloperoxidase-derived oxidants: differential biological effects of hypochlorous and hypothiocyanous acids. Free Radic Res. 2012;46(8):975–95. doi: 10.3109/10715762.2012.667566. [PubMed: 22348603]
82. van Dalen CJ, Whitehouse MW, Winterbourn CC, Kettle AJ. Thiocyanate and chloride as competing substrates for myeloperoxidase. Biochem J. 1997;327 (Pt 2):487–201392. [PubMed: 9359420]
83. Zheng L, Settle M, Brubaker G, Schmitt D, Hazen SL, Smith JD, et al. Localization of nitration and chlorination sites on apolipoprotein A-I catalyzed by myeloperoxidase in human atheroma and associated oxidative impairment in ABCA1-dependent cholesterol efflux from macrophages. J Biol Chem. 2005;280(1):38–47. 10.1074/jbc.M407019200. [PubMed: 15498770]
84. Ulmer TS, Bax A, Cole NB, Nussbaum RL. Structure and dynamics of micelle-bound human alpha-synuclein. J Biol Chem. 2005;280(10):9595–603. doi: 10.1074/jbc.M411805200. [PubMed: 15615727]
85. Rao JN, Jao CC, Hegde BG, Langen R, Ulmer TS. A combinatorial NMR and EPR approach for evaluating the structural ensemble of partially folded proteins. J Am Chem Soc. 2010;132(25):8657–68. doi: 10.1021/ja100646t. [PubMed: 20524659]
86. Hitti FL, Siegelbaum SA. The hippocampal CA2 region is essential for social memory. Nature. 2014;508(7494):88–92. doi: 10.1038/nature13028. [PubMed: 24572357]
87. DeVito LM, Konigsberg R, Lykken C, Sauvage M, Young WS 3rd, Eichenbaum H. Vasopressin 1b receptor knock-out impairs memory for temporal order. J Neurosci. 2009;29(9):2676–83. doi: 10.1523/JNEUROSCI.5488-08.2009. [PubMed: 19261862]
88. Piskorowski RA, Nasrallah K, Diamantopoulou A, Mukai J, Hassan SI, Siegelbaum SA, et al. Age-Dependent Specific Changes in Area CA2 of the Hippocampus and Social Memory Deficit in a Mouse Model of the 22q11.2 Deletion Syndrome. Neuron. 2016;89(1):163–76. doi: 10.1016/j.neuron.2015.11.036. [PubMed: 26748091]
89. Churchyard A, Lees AJ. The relationship between dementia and direct involvement of the hippocampus and amygdala in Parkinson's disease. Neurology. 1997;49(6):1570–6. [PubMed: 9409348]
90. Kohara K, Pignatelli M, Rivest AJ, Jung HY, Kitamura T, Suh J, et al. Cell type-specific genetic and optogenetic tools reveal hippocampal CA2 circuits. Nat Neurosci. 2014;17(2):269–79. doi: 10.1038/nn.3614. [PubMed: 24336151]

91. Dudek SM, Alexander GM, Farris S. Rediscovering area CA2: unique properties and functions. Nat Rev Neurosci. 2016;17(2):89–102. doi: 10.1038/nrn.2015.22. [PubMed: 26806628]
92. Hetz C, Papa FR. The Unfolded Protein Response and Cell Fate Control. Mol Cell. 2018;69(2): 169–81. doi: 10.1016/j.molcel.2017.06.017. [PubMed: 29107536]
93. Casciaro M, Di Salvo E, Pace E, Ventura-Spagnolo E, Navarra M, Gangemi S. Chlorinative stress in age-related diseases: a literature review. Immun Ageing. 2017;14:21. doi: 10.1186/s12979-017-0104-5. [PubMed: 29163665]
94. Saed GM, Ali-Fehmi R, Jiang ZL, Fletcher NM, Diamond MP, Abu-Soud HM, et al. Myeloperoxidase serves as a redox switch that regulates apoptosis in epithelial ovarian cancer. Gynecol Oncol. 2010;116(2):276–81. doi: 10.1016/j.ygyno.2009.11.004. [PubMed: 19962178]
95. Schabath MB, Spitz MR, Delclos GL, Gunn GB, Whitehead LW, Wu X. Association between asbestos exposure, cigarette smoking, myeloperoxidase (MPO) genotypes, and lung cancer risk. Am J Ind Med. 2002;42(1):29–37. doi: 10.1002/ajim.10084. [PubMed: 12111688]
96. Bell JS, Spencer JI, Yates RL, Yee SA, Jacobs BM, DeLuca GC. Invited Review: From nose to gut - the role of the microbiome in neurological disease. Neuropathol Appl Neurobiol. 2018. doi: 10.1111/nan.12520.
97. Dominy SS, Lynch C, Ermini F, Benedyk M, Marczyk A, Konradi A, et al. Porphyromonas gingivalis in Alzheimer's disease brains: Evidence for disease causation and treatment with small-molecule inhibitors. Sci Adv. 2019;5(1):eaau3333. doi: 10.1126/sciadv.aau3333. [PubMed: 30746447]
98. Boveris A, Chance B. The mitochondrial generation of hydrogen peroxide. General properties and effect of hyperbaric oxygen. Biochem J. 1973;134(3):707–16. [PubMed: 4749271]
99. Adam-Vizi V Production of reactive oxygen species in brain mitochondria: contribution by electron transport chain and non-electron transport chain sources. Antioxid Redox Signal. 2005;7(9–10):1140–9. doi: 10.1089/ars.2005.7.1140. [PubMed: 16115017]
100. Edmondson DE, Binda C. Monoamine Oxidases. Subcell Biochem. 2018;87:117–39. doi: 10.1007/978-981-10-7757-9_5. [PubMed: 29464559]
101. Lambeth JD. NOX enzymes and the biology of reactive oxygen. Nat Rev Immunol. 2004;4(3): 181–9. doi: 10.1038/nri1312. [PubMed: 15039755]
102. Belarbi K, Cuvelier E, Destee A, Gressier B, Chartier-Harlin MC. NADPH oxidases in Parkinson's disease: a systematic review. Mol Neurodegener. 2017;12(1):84. doi: 10.1186/s13024-017-0225-5. [PubMed: 29132391]
103. Hsu LJ, Sagara Y, Arroyo A, Rockenstein E, Sisk A, Mallory M, et al. alpha-synuclein promotes mitochondrial deficit and oxidative stress. Am J Pathol. 2000;157(2):401–10. [PubMed: 10934145]
104. Wu DC, Teismann P, Tieu K, Vila M, Jackson-Lewis V, Ischiropoulos H, et al. NADPH oxidase mediates oxidative stress in the 1-methyl-4-phenyl-1,2,3,6-tetrahydropyridine model of Parkinson's disease. Proc Natl Acad Sci U S A. 2003;100(10):6145–50. doi: 10.1073/pnas.0937239100. [PubMed: 12721370]
105. Wang Q, Qian L, Chen SH, Chu CH, Wilson B, Oyarzabal E, et al. Post-treatment with an ultra-low dose of NADPH oxidase inhibitor diphenyleneiodonium attenuates disease progression in multiple Parkinson's disease models. Brain. 2015;138(Pt 5):1247–62. doi: 10.1093/brain/awv034. [PubMed: 25716193]
106. Hou L, Sun F, Huang R, Sun W, Zhang D, Wang Q. Inhibition of NADPH oxidase by apocynin prevents learning and memory deficits in a mouse Parkinson's disease model. Redox Biol. 2019;22:101134. doi: 10.1016/j.redox.2019.101134. [PubMed: 30798073]
107. Winterbourn CC, Kettle AJ. Biomarkers of myeloperoxidase-derived hypochlorous acid. Free Radic Biol Med. 2000;29(5):403–9. [PubMed: 11020661]
108. Jeitner TM, Kalogiannis M, Krasnikov BF, Gomolin I, Peltier MR, Moran GR. Linking Inflammation and Parkinson Disease: Hypochlorous Acid Generates Parkinsonian Poisons. Toxicol Sci. 2016;151(2):388–402. doi: 10.1093/toxsci/kfw052. [PubMed: 27026709]
109. Mehta NJ, Asmaro K, Hermiz DJ, Njus MM, Saleh AH, Beningo KA, et al. Hypochlorite converts cysteinyl-dopamine into a cytotoxic product: A possible factor in Parkinson's Disease.

Free Radic Biol Med. 2016;101:44–52. doi: 10.1016/j.freeradbiomed.2016.09.023. [PubMed: 27682361]

110. Jacob JS, Cistola DP, Hsu FF, Muzaffar S, Mueller DM, Hazen SL, et al. Human phagocytes employ the myeloperoxidase-hydrogen peroxide system to synthesize dityrosine, trityrosine, pulcherosine, and isodityrosine by a tyrosyl radical-dependent pathway. J Biol Chem. 1996;271(33):19950–6. [PubMed: 8702710]
111. Beckman JS, Koppenol WH. Nitric oxide, superoxide, and peroxynitrite: the good, the bad, and ugly. Am J Physiol. 1996;271(5 Pt 1):C1424–37. doi: 10.1152/ajpcell.1996.271.5.C1424. [PubMed: 8944624]
112. Eiserich JP, Hristova M, Cross CE, Jones AD, Freeman BA, Halliwell B, et al. Formation of nitric oxide-derived inflammatory oxidants by myeloperoxidase in neutrophils. Nature. 1998;391(6665):393–7. doi: 10.1038/34923. [PubMed: 9450756]
113. Klebanoff SJ. Reactive nitrogen intermediates and antimicrobial activity: role of nitrite. Free Radic Biol Med. 1993;14(4):351–60. [PubMed: 8385644]
114. Delanghe S, Delanghe JR, Speeckaert R, Van Biesen W, Speeckaert MM. Mechanisms and consequences of carbamoylation. Nat Rev Nephrol. 2017;13(9):580–93. doi: 10.1038/nrneph.2017.103. [PubMed: 28757635]
115. Wang Z, Nicholls SJ, Rodriguez ER, Kummu O, Horkko S, Barnard J, et al. Protein carbamylation links inflammation, smoking, uremia and atherogenesis. Nat Med. 2007;13(10):1176–84. doi: 10.1038/nm1637. [PubMed: 17828273]
116. Holzer M, Gauster M, Pfeifer T, Wadsack C, Fauler G, Stiegler P, et al. Protein carbamylation renders high-density lipoprotein dysfunctional. Antioxid Redox Signal. 2011;14(12):2337–46. doi: 10.1089/ars.2010.3640. [PubMed: 21235354]
117. Nagahara N, Okazaki T, Nishino T. Cytosolic mercaptopyruvate sulfurtransferase is evolutionarily related to mitochondrial rhodanese. Striking similarity in active site amino acid sequence and the increase in the mercaptopyruvate sulfurtransferase activity of rhodanese by site-directed mutagenesis. J Biol Chem. 1995;270(27):16230–5. [PubMed: 7608189]
118. Delporte C, Zouaoui Boudjeltia K, Furtmuller PG, Maki RA, Dieu M, Noyon C, et al. Myeloperoxidase-catalyzed oxidation of cyanide to cyanate: A potential carbamylation route involved in the formation of atherosclerotic plaques? J Biol Chem. 2018;293(17):6374–86. doi: 10.1074/jbc.M117.801076. [PubMed: 29496995]
119. Wagner BA, Reszka KJ, McCormick ML, Britigan BE, Evig CB, Burns CP. Role of thiocyanate, bromide and hypobromous acid in hydrogen peroxide-induced apoptosis. Free Radic Res. 2004;38(2):167–75. [PubMed: 15104210]
120. Chandler JD, Day BJ. Biochemical mechanisms and therapeutic potential of pseudohalide thiocyanate in human health. Free Radic Res. 2015;49(6):695–710. doi: 10.3109/10715762.2014.1003372. [PubMed: 25564094]
121. Skaff O, Pattison DI, Davies MJ. Hypothiocyanous acid reactivity with low-molecular-mass and protein thiols: absolute rate constants and assessment of biological relevance. Biochem J. 2009;422(1): 111–7. doi: 10.1042/BJ20090276. [PubMed: 19492988]
122. Talib J, Pattison DI, Harmer JA, Celermajer DS, Davies MJ. High plasma thiocyanate levels modulate protein damage induced by myeloperoxidase and perturb measurement of 3-chlorotyrosine. Free Radic Biol Med. 2012;53(1):20–9. doi: 10.1016/j.freeradbiomed.2012.04.018. [PubMed: 22609005]
123. Chandler JD, Min E, Huang J, Nichols DP, Day BJ. Nebulized thiocyanate improves lung infection outcomes in mice. Br J Pharmacol. 2013;169(5): 1166–77. doi: 10.1111/bph.12206. [PubMed: 23586967]
124. Morgan PE, Laura RP, Maki RA, Reynolds WF, Davies MJ. Thiocyanate supplementation decreases atherosclerotic plaque in mice expressing human myeloperoxidase. Free Radic Res. 2015;49(6):743–9. doi: 10.3109/10715762.2015.1019347. [PubMed: 25812586]
125. Bafort F, Parisi O, Perraudin JP, Jijakli MH. Mode of action of lactoperoxidase as related to its antimicrobial activity: a review. Enzyme Res. 2014;2014:517164. doi: 10.1155/2014/517164. [PubMed: 25309750]

126. Sarr D, Toth E, Gingerich A, Rada B. Antimicrobial actions of dual oxidases and lactoperoxidase. J Microbiol. 2018;56(6):373–86. doi: 10.1007/s12275-018-7545-1. [PubMed: 29858825]

127. Morrison M, Allen PZ. Lactoperoxidase: identification and isolation from Harderian and lacrimal glands. Science. 1966;152(3729):1626–8. [PubMed: 4956921]

128. Ueda T, Sakamaki K, Kuroki T, Yano I, Nagata S. Molecular cloning and characterization of the chromosomal gene for human lactoperoxidase. Eur J Biochem. 1997;243(1–2):32–41. [PubMed: 9030719]

129. Wu X, Zheng T, Zhang B. Exosomes in Parkinson's Disease. Neurosci Bull. 2017;33(3):331–8. doi: 10.1007/s12264-016-0092-z. [PubMed: 28025780]

130. Moguilevsky N, Garcia-Quintana L, Jacquet A, Tournay C, Fabry L, Pierard L, et al. Structural and biological properties of human recombinant myeloperoxidase produced by Chinese hamster ovary cell lines. Eur J Biochem. 1991; 197(3):605–14. [PubMed: 1851479]

131. Nauseef WM, Cogley M, McCormick S. Effect of the R569W missense mutation on the biosynthesis of myeloperoxidase. J Biol Chem. 1996;271(16):9546–9. [PubMed: 8621627]

132. Grishkovskaya T, Paumann-Page M, Tscheliessnig R, Stampler J, Hofbauer S, Soudi M, et al. Structure of human promyeloperoxidase (proMPO) and the role of the propeptide in processing and maturation. J Biol Chem. 2017;292(20):8244–61. doi: 10.1074/jbc.M117.775031. [PubMed: 28348079]

133. Olsen RL, Steigen TK, Holm T, Little C. Molecular forms of myeloperoxidase in human plasma. Biochem J. 1986;237(2):559–65. [PubMed: 3026323]

134. Khalilova TS, Dickerhof N, Mocatta TJ, Bhagra CJ, McClean DR, Obinger C, et al. A myeloperoxidase precursor, pro-myeloperoxidase, is present in human plasma and elevated in cardiovascular disease patients. PLoS One. 2018;13(3):e0192952. doi: 10.1371/journal.pone.0192952. [PubMed: 29590135]

135. Nauseef WM. Myeloperoxidase biosynthesis by a human promyelocytic leukemia cell line: insight into myeloperoxidase deficiency. Blood. 1986;67(4):865–72. [PubMed: 3006833]

136. Yamada M, Hur SJ, Toda H. Tsolation and characterization of extracellular myeloperoxidase precursor in HL-60 cell cultures. Biochem Biophys Res Commun. 1990;166(2):852–9. [PubMed: 2154223]

137. Tobler A, Miller CW, Johnson KR, Selsted ME, Rovera G, Koeffler HP. Regulation of gene expression of myeloperoxidase during myeloid differentiation. J Cell Physiol. 1988;136(2):215–25. doi: 10.1002/jcp.1041360203. [PubMed: 2842344]

138. Lin KM, Austin GE. Functional activity of three distinct myeloperoxidase (MPO) promoters in human myeloid cells. Leukemia. 2002;16(6):1143–53. doi: 10.1038/sj.leu.2402514. [PubMed: 12040446]

139. Orita T, Shimozaki K, Murakami H, Nagata S. Binding of NF-Y transcription factor to one of the cis-elements in the myeloperoxidase gene promoter that responds to granulocyte colony-stimulating factor. J Biol Chem. 1997;272(37):23216–23. [PubMed: 9287329]

140. Vanhamme L, Zouaoui Boudjeltia K, Van Antwerpen P, Delporte C. The other myeloperoxidase: Emerging functions. Arch Biochem Biophys. 2018;649:1–14. doi: 10.1016/j.abb.2018.03.037. [PubMed: 29614255]

141. Roumeguere T, Delree P, Van Antwerpen P, Rorive S, Vanhamme L, de Ryhove Lde L, et al. Tntriguing location of myeloperoxidase in the prostate: a preliminary immunohistochemical study. Prostate. 2012;72(5):507–13. doi: 10.1002/pros.21452. [PubMed: 21739466]

142. Khalil A, Medfai H, Poelvoorde P, Kazan MF, Delporte C, Van Antwerpen P, et al. Myeloperoxidase promotes tube formation, triggers ERK1/2 and Akt pathways and is expressed endogenously in endothelial cells. Arch Biochem Biophys. 2018;654:55–69. doi: 10.1016/j.abb.2018.07.011. [PubMed: 30016634]

143. Wang Y, Chen XY, Wang K, Li S, Zhang XY. Myeloperoxidase polymorphism and coronary artery disease risk: A meta-analysis. Medicine (Baltimore). 2017;96(27):e7280. doi: 10.1097/MD.0000000000007280. [PubMed: 28682877]

144. Yang WJ, Wang MY, Pan FZ, Shi C, Cen H. Association between MPO-463G > A polymorphism and cancer risk: evidence from 60 case-control studies. World J Surg Oncol. 2017;15(1): 144. doi: 10.1186/s12957-017-1183-7. [PubMed: 28764808]

145. Cabral-Miranda F, Hetz C. ER Stress and Neurodegenerative Disease: A Cause or Effect Relationship? Curr Top Microbiol Immunol. 2018;414:131–57. doi: 10.1007/82_2017_52. [PubMed: 28864830]

146. Hoozemans JJ, van Haastert ES, Eikelenboom P, de Vos RA, Rozemuller JM, Scheper W. Activation of the unfolded protein response in Parkinson's disease. Biochem Biophys Res Commun. 2007;354(3):707–11. doi: 10.1016/j.bbrc.2007.01.043. [PubMed: 17254549]

147. Bellucci A, Navarria L, Zaltieri M, Falarti E, Bodei S, Sigala S, et al. Induction of the unfolded protein response by alpha-synuclein in experimental models of Parkinson's disease. J Neurochem. 2011;116(4):588–605. doi: 10.1111/j.1471-4159.2010.07143.x. [PubMed: 21166675]

148. Colla E, Jensen PH, Pletnikova O, Troncoso JC, Glabe C, Lee MK. Accumulation of toxic alpha-synuclein oligomer within endoplasmic reticulum occurs in alpha-synucleinopathy in vivo. J Neurosci. 2012;32(10):3301–5. doi: 10.1523/JNEUROSCI.5368-11.2012. [PubMed: 22399752]

149. Colla E, Coune P, Liu Y, Pletnikova O, Troncoso JC, Iwatsubo T, et al. Endoplasmic reticulum stress is important for the manifestations of alpha-synucleinopathy in vivo. J Neurosci. 2012;32(10):3306–20. doi: 10.1523/JNEUROSCI.5367-11.2012. [PubMed: 22399753]

150. Belal C, Ameli NJ, El Kommos A, Bezalel S, Al'Khafaji AM, Mughal MR, et al. The homocysteine-inducible endoplasmic reticulum (ER) stress protein Herp counteracts mutant alpha-synuclein-induced ER stress via the homeostatic regulation of ER-resident calcium release channel proteins. Hum Mol Genet. 2012;21(5):963–77. doi: 10.1093/hmg/ddr502. [PubMed: 22045699]

151. Baleriola J, Walker CA, Jean YY, Crary JF, Troy CM, Nagy PL, et al. Axonally synthesized ATF4 transmits a neurodegenerative signal across brain regions. Cell. 2014; 158(5): 1159–72. doi: 10.1016/j.cell.2014.07.001. [PubMed: 25171414]

152. Irwin DJ, Lee VM, Trojanowski JQ. Parkinson's disease dementia: convergence of alpha-synuclein, tau and amyloid-beta pathologies. Nat Rev Neurosci. 2013;14(9):626–36. doi: 10.1038/nrn3549. [PubMed: 23900411]

153. Peng C, Gathagan RJ, Lee VM. Distinct alpha-Synuclein strains and implications for heterogeneity among alpha-Synucleinopathies. Neurobiol Dis. 2018;109(Pt B):209–18. doi: 10.1016/j.nbd.2017.07.018. [PubMed: 28751258]

154. Pang CC, Kiecker C, O'Brien JT, Noble W, Chang RC. Ammon's Horn 2 (CA2) of the Hippocampus: A Long-Known Region with a New Potential Role in Neurodegeneration. Neuroscientist. 2018:10.1177/1073858418778747.

155. Kim H, Gearing M, Mirra SS. Ubiquitin-positive CA2/3 neurites in hippocampus coexist with cortical Lewy bodies. Neurology. 1995;45(9):1768–70. [PubMed: 7675245]

156. Flores-Cuadrado A, Ubeda-Banon I, Saiz-Sanchez D, de la Rosa-Prieto C, Martinez-Marcos A. Hippocampal alpha-synuclein and interneurons in Parkinson's disease: Data from human and mouse models. Mov Disord. 2016;31(7):979–88. doi: 10.1002/mds.26586. [PubMed: 26991075]

157. Adamowicz DH, Roy S, Salmon DP, Galasko DR, Hansen LA, Masliah E, et al. Hippocampal alpha-Synuclein in Dementia with Lewy Bodies Contributes to Memory Impairment and Is Consistent with Spread of Pathology. J Neurosci. 2017;37(7):1675–84. doi: 10.1523/JNEUROSCI.3047-16.2016. [PubMed: 28039370]

158. Jucaite A, Svenningsson P, Rinne JO, Cselenyi Z, Varnas K, Johnstrom P, et al. Effect of the myeloperoxidase inhibitor AZD3241 on microglia: a PET study in Parkinson's disease. Brain. 2015;138(Pt 9):2687–700. doi: 10.1093/brain/awv184. [PubMed: 26137956]

159. Zhang H, Ray A, Miller NM, Hartwig D, Pritchard KA, Dittel BN. Inhibition of myeloperoxidase at the peak of experimental autoimmune encephalomyelitis restores blood-brain barrier integrity and ameliorates disease severity. J Neurochem. 2016;136(4):826–36. doi: 10.1111/jnc.13426. [PubMed: 26560636]

160. Stefanova N, Georgievska B, Eriksson H, Poewe W, Wenning GK. Myeloperoxidase inhibition ameliorates multiple system atrophy-like degeneration in a transgenic mouse model. Neurotox Res. 2012;21(4):393–404. doi: 10.1007/s12640-011-9294-3. [PubMed: 22161470]

161. Kaindlstorfer C, Sommer P, Georgievska B, Mather RJ, Kugler AR, Poewe W, et al. Failure of Neuroprotection Despite Microglial Suppression by Delayed-Start Myeloperoxidase Inhibition in

a Model of Advanced Multiple System Atrophy: Clinical Implications. Neurotox Res. 2015;28(3):185–94. doi: 10.1007/s12640-015-9547-7. [PubMed: 26194617]

Highlights

- Human MPO transgene is expressed in neurons in the A53T-αSyn model of PD
- hMPO colocalizes in neurons with nitrated and carbamylated αSyn and HOCl epitopes
- hMPO in A53T brain is primarily the precursor proMPO that can be secreted
- hMPO-A53T mouse has worse motor impairment on rotarod, balance beam and wire hang
- In PD SN, MPO is expressed in neurons with nitrated αSyn and HOCl modified proteins

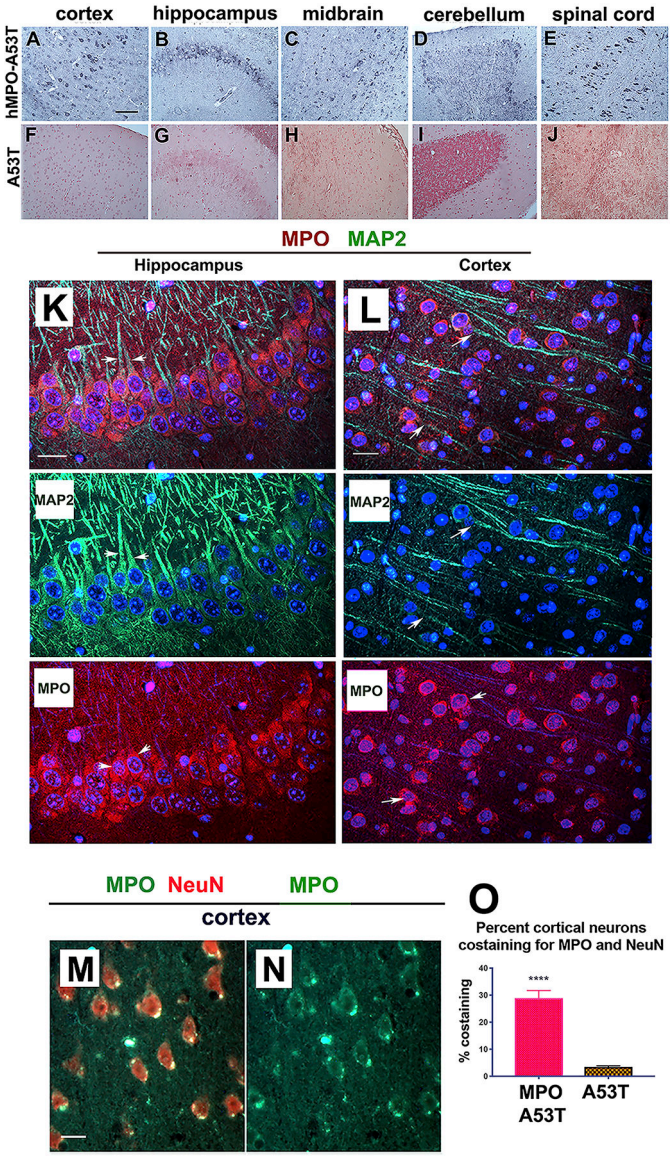

Figure 1. hMPO is expressed in neurons in the hMPO-A53T mouse model of PD.

(A-E) Representative photomicrographs showing MPO immunostaining in brain sections from the hMPO-A53T mice in (A) cortex, (B) hippocampus, (C) midbrain, (D) cerebellum and (E) spinal cord. (F – J) The same regions of A53T brain sections were immunostained for MPO. Due to low levels of immunostaining for mouse MPO, sections F-J were stained with nuclear fast red to show tissue architecture. Scale bar for A-J is in panel A (50 mm). (K and L) Representative dual color photomicrograph of immunofluorescence staining of MPO (red) and MAP2 (green) in hippocampal (K) and cortical (L) regions from the hMPO-A53T mouse. Single channel images for the green or red fluorescence are shown below the merged images. Arrows indicate green MAP2 stained projections extending from red MPO stained soma in both hippocampus (K) and cortex (L). Scale bars for K and L are 10 μm. (M) Representative immunofluorescence staining of MPO (green) and NeuN (red) in the cortex. (N) Single channel green immunofluorescence staining of MPO in the cortex. (O)

Image analysis of representative sections to estimate the percent of cells showing colocalization with MPO and NeuN. Scale bar for M,N is in M (10 μm). All mice used in these studies were males.

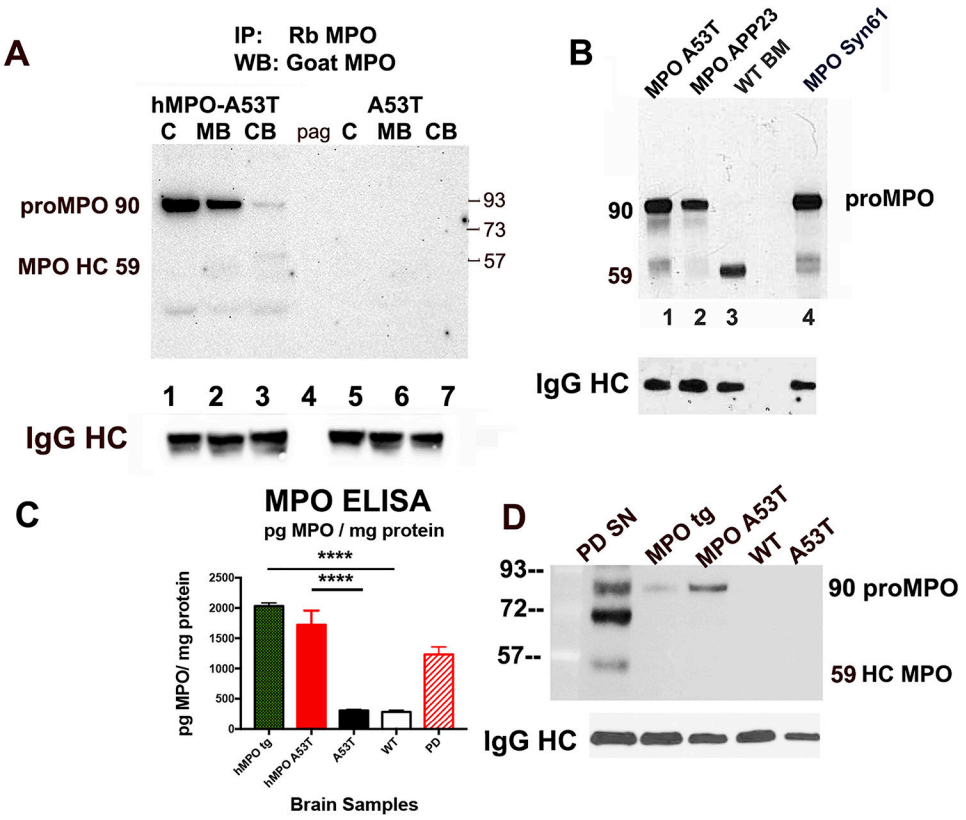

Figure 2. MPO is expressed as the precursor 90 kDa Pro-MPO secretory form

(A). Immunoprecipitation of MPO from different brain regions. Antibodies to MPO (DAKO, rabbit) were added to extracts of isolated regions of mouse brains and bound proteins pulled down with magnetic protein A/G beads. Bound proteins were eluted and fractionated by SDS-PAGE (4–12%). Western blots were probed with HRP-conjugated goat anti-MPO antibodies (R&D) to reveal immunoprecipitated proteins from hMPO-A53T cortex/ hippocampus (C) (lane1), midbrain including thalamus, striatum, substantia nigra (MB) (lane 2), or cerebellum/brainstem (CB) (lane 3). The control pulldown from the hMPO-A53T cortical extract with Protein A/G beads in absence of antibodies to MPO is in lane 4 (pag). Proteins were also pulled down from extracts of A53T cortex (C) (lane 5), midbrain (MB) (lane 6), and cerebellum/brainstem (CB) (lane 7). (n= 4 MPO-A53T brains and 4 A53T brains separated into cortex/hippocampus, midbrain, and cerebellum/brainstem, the regions combined and extracts prepared for immunoprecipitation). The Western blot was probed for rabbit IgG heavy chain as a loading control (IgG HC).

(B) Immunoprecipitation of MPO from brain of other mouse strains revealed that proMPO is predominantly expressed in several mouse models in which the humanized MPO mouse was crossed to neurodegenerative disease models including the PD model expressing A53T (MPO-A53T) (lane1), an AD model expressing the human amyloid precursor protein (MPO-APP23) (lane 2), and the PD model expressing wild-type (WT) hαSyn (MPO-Syn61) (lane 4). Mouse WT bone marrow (WT BM) (lane 3) was included as a myeloid control expressing the MPO 59 kDa heavy chain. The Western blot was probed for rabbit IgG heavy chain as a loading control (IgG HC).

(C) MPO was quantified by ELISA in brain extracts prepared from hMPO tg, hMPO-A53T, A53T, C57Bl/6 WT and human PD SN. Protein levels were determined by BCA. For the mouse samples each bar represents the average +/− S.E.M. (n=6). For the human PD samples the bar represents the average +/− S.E.M. (n=3). The mouse data were analyzed using one-way ANOVA with post hoc Dunnett's test. The asterisks indicate a significant difference ($p<0.0001$) between the hMPO tg and hMPO-A53T as compared to A53T or C57Bl/6 WT mice.

(D) MPO was immunoprecipitated as above from human PD SN and compared to hMPO tg, MPO-A53T, WT, and A53T whole brain extracts. The proMPO 90 kDa band is present in PD SN comigrating with the 90 kDa band in hMPO tg and MPO-A53T, but lacking in WT and A53T brain. The PD SN sample also had the 55–59 kDa MPO heavy chain as well as a 70 kDa band which may be a processing intermediate. The Western blot was probed for rabbit IgG heavy chain as a loading control (IgG HC). All mice used in these studies were males.

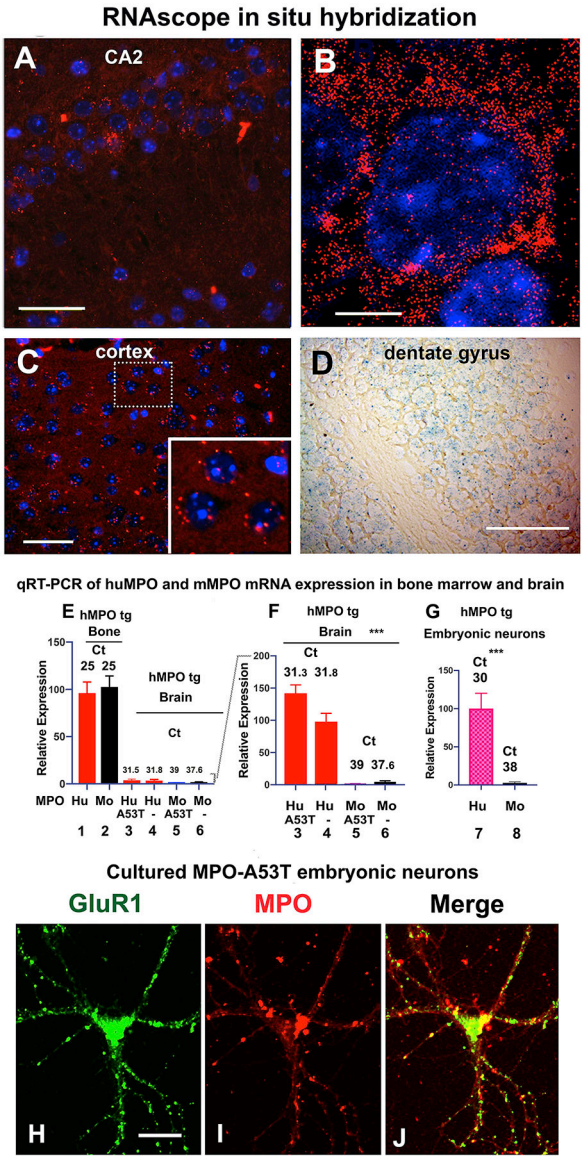

Figure 3. hMPO mRNA is expressed in neurons in the hMPO-A53T mice while mMPO mRNA is low to nondetectable.

(A)Immunofluorescence detection of hMPO mRNA transcripts in puncta in CA2 neurons of the hMPO-A53T mice at low power (AlexaFluor 594, red) as detected by RNAscope *in situ* hybridization. (B) Higher resolution confocal image of a single central CA2 neuron with an oil immersion 63x objective showing distinct puncta of hMPO mRNA (red) with nuclei counterstained with DAPI. (C) hMPO mRNA transcripts detected in cortical neurons of the hMPO-A53T mice with boxed area enlarged at corner. (D) hMPO mRNA detected by blue peroxidase chromagen over dentate gyrus neurons at low magnification. Scale bar A (30 μm); B (5 μm); (C 40 μm); D (30 μm). H,I,J (10 μm). (E,F) qPCR measures hMPO mRNA and mMPO mRNA extracted from bone marrow or brains of hMPO transgenic or hMPO-A53T mice. hMPO expression in hMPO A53T bone marrow is set at 100 on the relative scale (E) with the quantitation cycle (Ct) of Ct 25 for hMPO (lane 1) and Ct 25 for mMPO (lane 2). In brain tissue mRNA levels declined considerably (E lanes 3–6 enlarged in F with

hMPO (lane 4) set at 100 on the relative scale). hMPO expression is at Ct 31.3 in hMPO-A53T brain and 31.8 in hMPO transgenic brain (lanes 3 and 4). Mouse MPO expression is at Ct 39 in hMPO-A53T brain and Ct 37.6 in hMPO transgenic brain (lanes 5 and 6). Each increase of one Ct is equal to a twofold decrease in expression levels. Results were analyzed using GraphPad Prism ANOVA.

(G) In embryonic cultured neurons, hMPO mRNA expression was at Ct 30 (lane 7), similar to expression levels in brain (lane 4) while mMPO expression was at Ct 38 (lane 8), equivalent to levels in brain (lane 6). The qPCR results are shown as the mean Ct ± S.E.M. of three independent experiments performed in duplicate. Results in panel G were analyzed using GraphPad Prism and Student's t-test. (H-J) Immunostaining of a cultured embryonic neuron from MPO-A53T model showing neuron marker GluR1 (H), MPO (I), and the merged image showing colocalization (J). Scale bar 10 μm. All mice used in these studies were males.

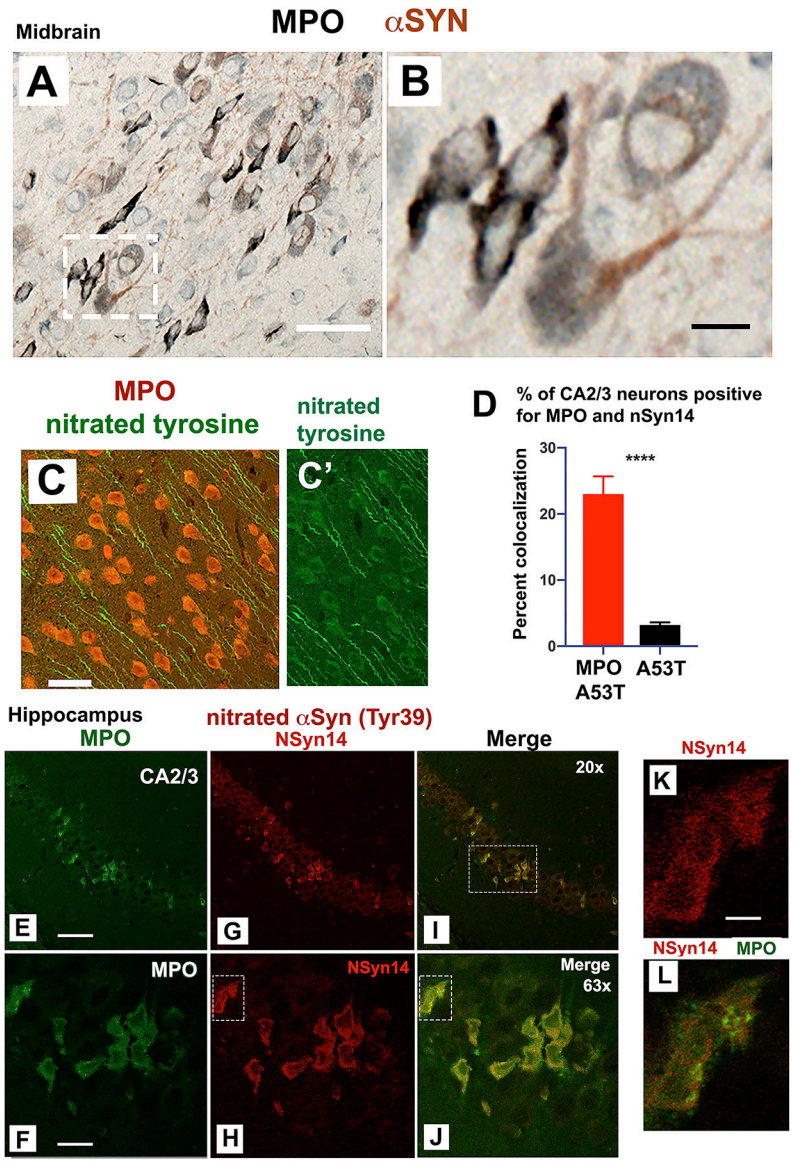

Figure 4. hMPO expression in neurons in the hMPO-A53T model is associated with increased nitration of αSyn.

(A) Immunostaining of dystrophic midbrain neurons containing αSyn (red, Syn505) and hMPO (black) (boxed region enlarged in B). (C) In cortical neurons, MPO is immunodetected in neuronal soma (red) while nitroTyr modified proteins are detected in neurite projections (green), seen more clearly in the single channel green (C'). (D) Quantitation of the percentage of hippocampal neurons in CA2/3 region that costain for both MPO and nSyn14 are shown for MPO A53T and A53T. (n = 3 mice of each genotype, three sections per brain, and 4 images per section were analyzed.)

(E-I) Immunostaining of the hippocampal CA2/3 region for MPO (E), nitrated αSyn (monoclonal antibody nSyn14 specific to nitrated αSyn) (G) and the merged image (I). Boxed area in panel I and the equivalent regions in E,G are enlarged below in F,H,J. The boxed area in merged J is enlarged in L (both MPO and nSyn14). The boxed area in H is enlarged in K (nSyn14 alone). All mice used in these studies were males.

Scale bar A (30 μm), B (10 μm), C and C' (30 μm), E,G,I (30 μm), F,H,J (10 μm), K,L (15 μm).

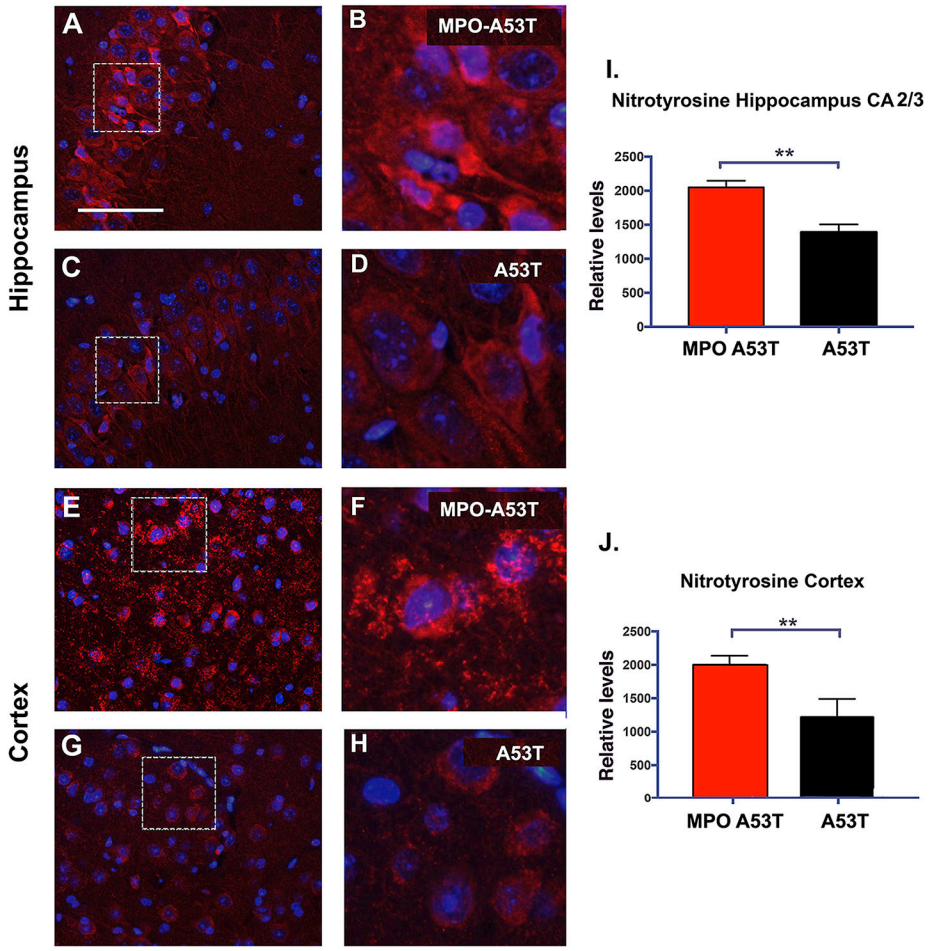

Figure 5. NitroTyr levels are higher in the hippocampus and cortex of hMPO-A53T mice as compared to the A53T mice.

(A,B,C,D) Immunohistochemical staining of nitroTyr in the hippocampus of the hMPO-A53T mice (A, boxed area enlarged in B) and the A53T mice (C, boxed area enlarged in D) (Millipore rabbit anti-nitrotyrosine, 1/200). (E,F,G,H) Immunohistochemical staining of nitroTyr in the cortex of the hMPO-A53T mice (E, enlarged in F) and the A53T mice (G, enlarged in H). (I,J) Quantitation of relative levels of nitrotyrosine staining in hippocampus (I) and in cortex (J). Fluorescence signal was measured as integrated density after background subtraction using Image J/Fiji software. Quantitation was performed on five biological replicates of each genotype using three paraffin sections of each, and analysis of four regions within each section of hippocampal CA2/3 and four regions from the cortex (** p <0.005, Student's t-test). Scale bar 30 mm. All mice used in these studies were males.

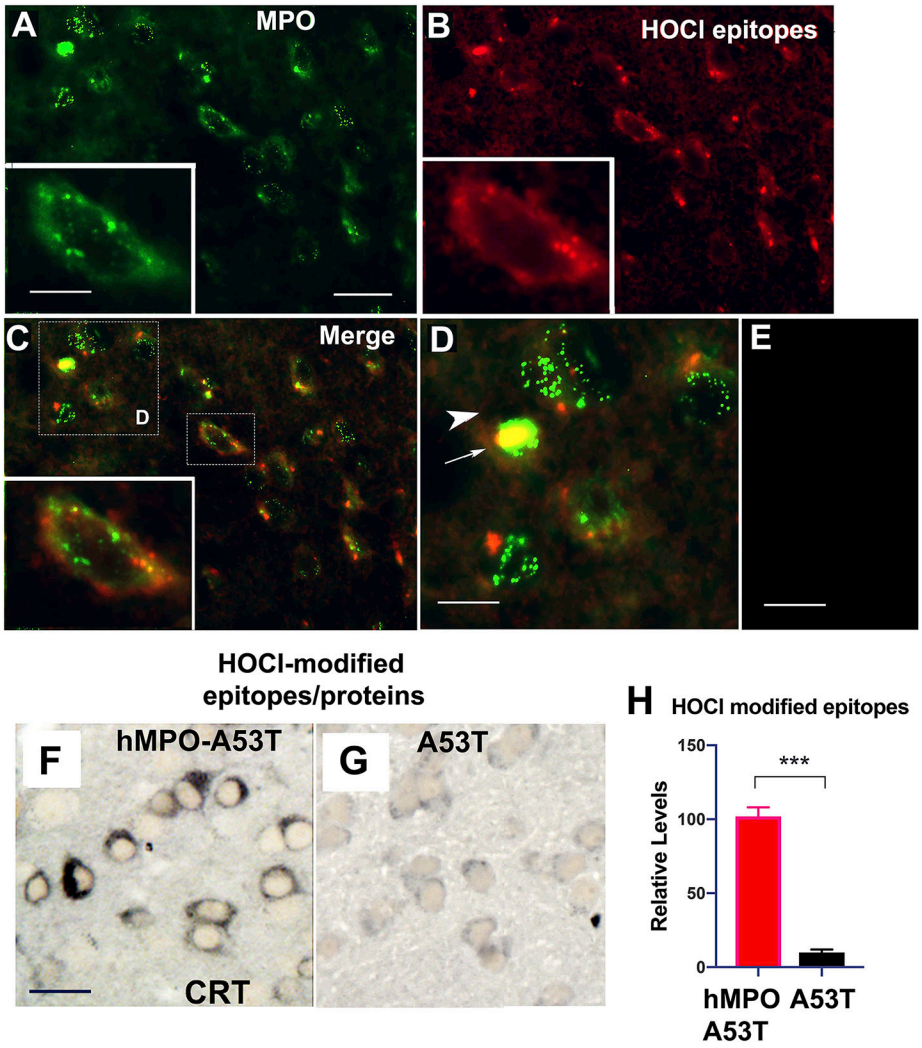

Figure 6. MPO colocalizes with HOCl-modified epitopes in hMPO-A53T brain.

(A)MPO immunostaining of cortical neurons in hMPO-A53T brain showing speckled vesicular pattern (AlexaFluor488, green). (B) Immunostaining for HOCl-modified epitopes using monoclonal antibody clone 2D10G9 (AlexaFluor 594, red). (C) Merged image with boxed central neuron enlarged at lower left inset, and same for panels A and B. (D) Left upper inset in panel C enlarged to show region of colocalization of HOCl epitopes and MPO (yellow, arrow) in neuron with unstained nucleus (arrowhead). The no primary antibody control image for merged green and red channels is shown in panel E. Scale bar A 10 mm. Scale bar insets 5 mm. Scale bar E 5 μm. Representative immunoperoxidase images show MPO-generated HOCl-modified epitopes detected in cortical neurons from MPO A53T (F) or A53T (G) with monoclonal antibody 2D10G9. (H) Image analysis of levels of 2D10G9 immunoreactivity expressed as corrected optical density analyzed by ImageJ/Fiji software (Student's t-test). N = 5 mice of each genotype, 3 sections analyzed, 4 images analyzed per section. All mice used in these studies were male.

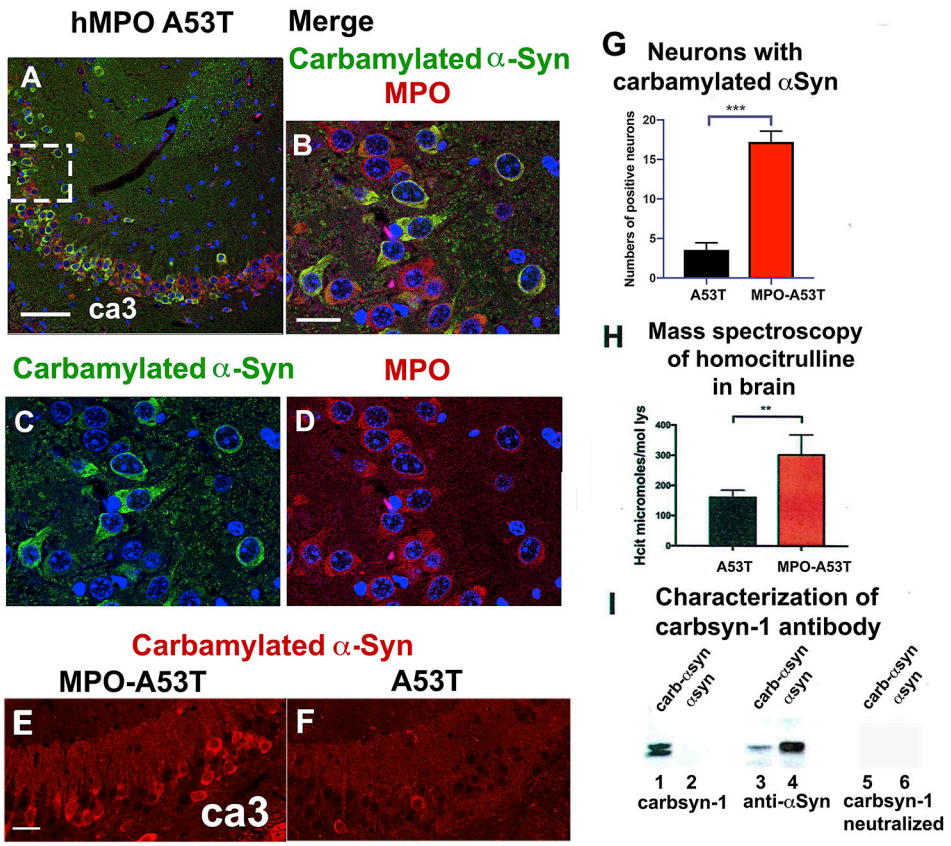

Figure 7. Carbamylated αSyn and MPO colocalize in hippocampal neurons of the hMPO-A53T mice.

(A)Immunostaining of MPO (red) and carbamylated αSyn (green) in mouse hippocampus (merged confocal image). (B) Boxed area in A is enlarged. (C) Green channel shows carbamylated αSyn alone. (D) Red channel shows MPO alone. (E,F) Carbamylated αSyn staining in MPO-A53T (E) and A53T (F) in the CA3 region of the hippocampus. (G) Quantitation of numbers of CA3 neurons positive for carbamylated αSyn in MPO-A53T and A53T hippocampus. (H) Mass spectrometry quantitation of levels of carbamylated lysine (homocitrulline) in the A53T mouse brain as compared to the hMPO-A53T mouse brain (**p <0.005). (I) Characterization of the carbsyn-1 antibody. The carbsyn-1 antibody recognizes carbamylated αSyn (Lane 1) but not αSyn (Lane 2). Both carbamylated αSyn and αSyn are recognized by the antibody to αSyn (BD). When the carbsyn-1 antibody was neutralized with a-Syn peptide #1 neither carbamylated αSyn (Lane 5) nor αSyn (Lane 6) were recognized by the carbsyn-1 antibody. For both carbamylated αSyn and αSyn, 0.2 micrograms of sample was loaded on the gel. Data represent mean ± S.E.M. (Student's t test. ***p <0.001). Scale bar A (50 μm), B-D (15 μm), E,F (10 μm). All mice used in these studies were male. N = 5 mice of each genotype, three sections from each brain, four images analyzed per section.

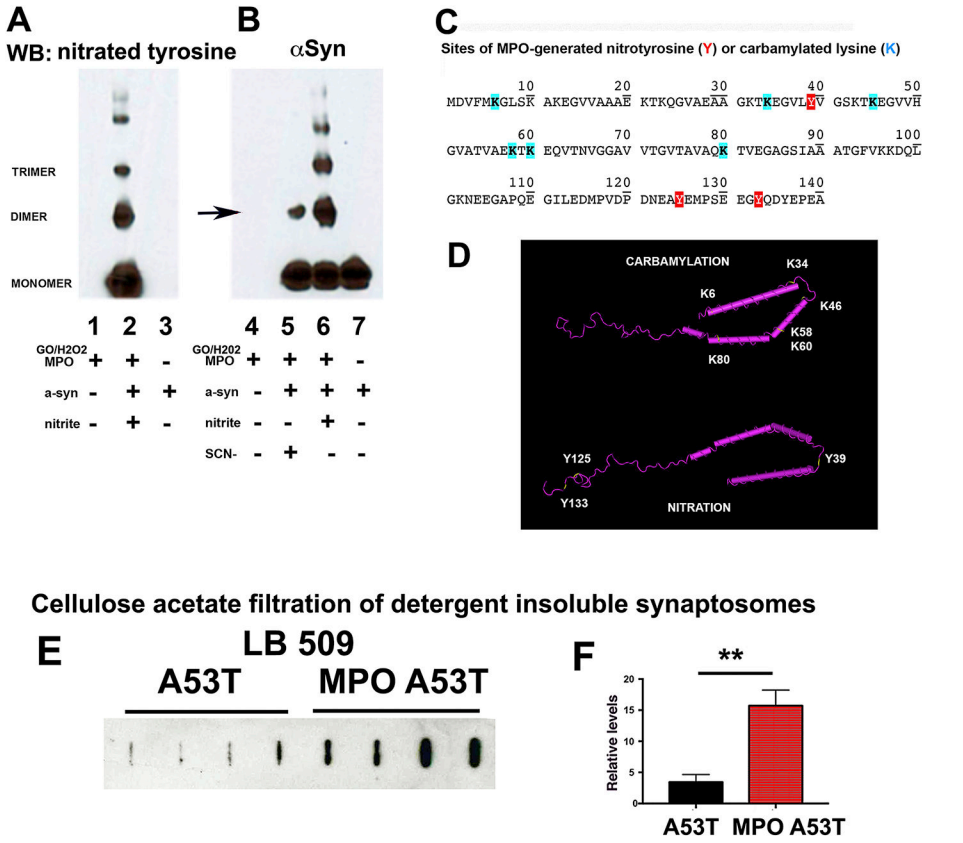

Figure 8. MPO nitrates and carbamylates αSyn *in vitro* giving rise to dimers and oligomers.

(A)(Lane 1–3) αSyn was incubated with MPO, glucose oxidase, and glucose (MPO-GO) and nitrite and subjected to SDS-PAGE (4–12%). Western blots were performed using an antibody to nitroTyr (Millipore) demonstrating the presence of nitrated monomer, dimers, trimers and oligomers (lane 2). The MPO-GO system (lane 1) or unmodified αSyn (lane 3) were used as controls. (B)(Lane 47) αSyn was incubated with the MPO-GO system in the presence of cyanate (SCN^-) (lane 5) or nitrite (lane 6). Samples were again subjected to SDS-PAGE and Western blots were performed using an affinity purified mAb to nonmodified αSyn (BD). Evidence of dimers was observed when αSyn was incubated with the MPO-GO system and SCN^- (lane 5) or dimers and oligomers when incubated with nitrite (lane 6). The MPO-GO system (lane 4) or unmodified αSyn (lane 7) were used as controls. (C) Schematic depiction of amino acid sequence of αSyn and identified sites of oxidation by MPO carbamylation (blue boxes) and nitration (red boxes) identified by mass spectrometry. (D) Model of carbamylation and nitration sites in αSyn (PDB ID:1XQ8) [84, 85]. (E) Synaptosome preparations from A53T and hMPO-A53T mouse brains were diluted in PBS + 1% NP40 for 1 h prior to mild suction through cellulose acetate filters (0.2 μm) and washed with PBS + 1% SDS prior to being probed with antibody LB509 that was generated against Lewy bodies and recognizes human but not mouse αSyn. Detection was with HRP labeled anti-mouse IgG. (F) Bar-graph of densitometric quantification of LB509 bands in E. Quantitation of band intensity was performed with Image Studio Lite software. Analysis of statistical significance was performed with GraphPad Prism (** $p < 0.001$, Student's t-test). All mice used in this study were males.

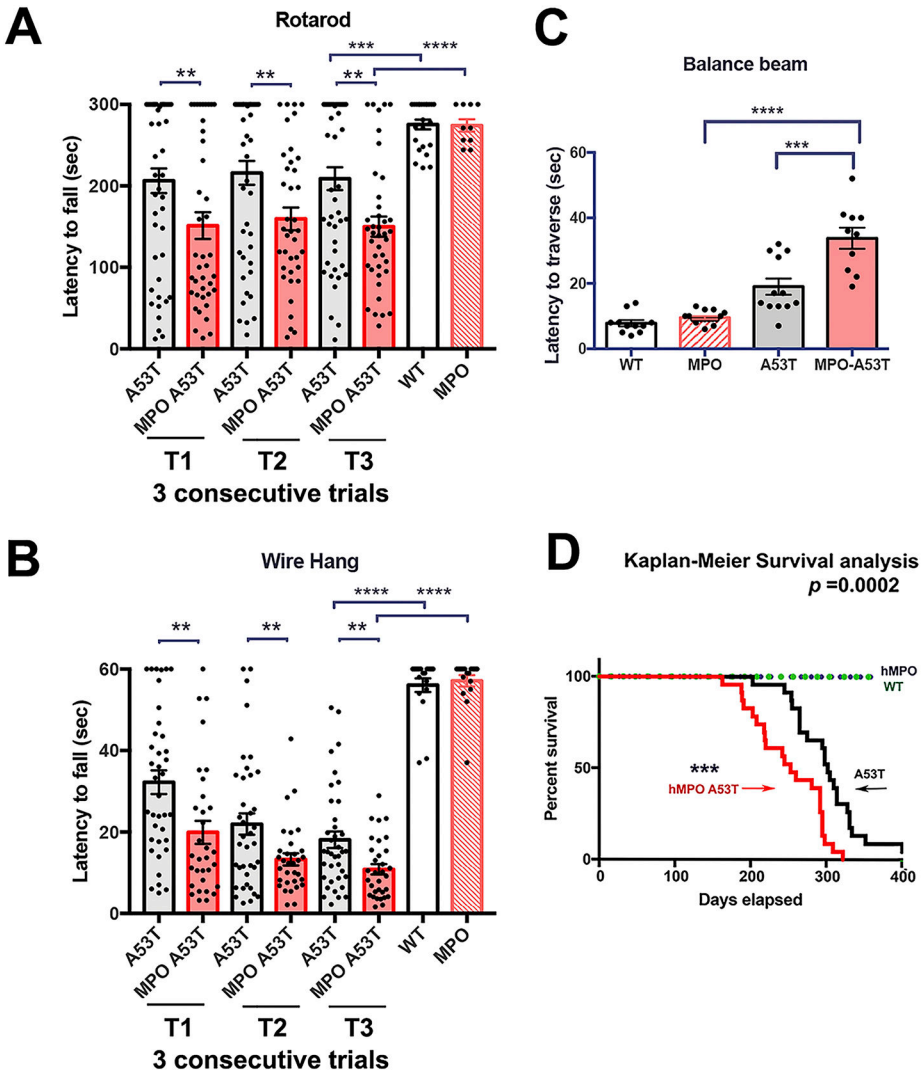

Figure 9. Impaired motor abilities in hMPO-A53T mice compared to A53T.

(A) Rotarod analysis was performed with the indicated genotypes A53T, hMPO-A53T, hMPO transgenics (MPO), and wild-type (WT, C57Bl/6) (n = 47 A53T, 40 hMPO-A53T, 10 hMPO, 23 WT). Only male mice were used in these experiments. Three consecutive trials (T1 – T3) with rest intervals were performed for each group. Only the third trial is shown for WT and hMPO mice. (B) The wire hang was performed with the indicated genotypes as in (A) (n = 38 A53T, 32 hMPO-A53T, 13 hMPO, 13 WT). Three trials with rest intervals were performed for each group. Only the third trial is shown for WT and MPO mice. (C) Balance beam was performed with the genotypes indicated (n = 6–11 for each group). Behavior data were analyzed using a one-way analysis of variance (ANOVA) followed by Dunnets post-hoc test using GraphPad Prism v8. Data are represented as mean +/− S.E.M. (**p, < 0.005, ***p, <0.001, ****p, <0.0001). (D) hMPO-A53T mice reach end stage paralysis earlier than A53T mice. This is shown for the hMPO-A53T, A53T, hMPO, and WT mice (n = 23 hMPO-A53T, 23 A53T, 10 hMPO, 10 WT). Onset of hind limb paralysis was the end point. Statistical significance determined by Kaplan-Meier survival analysis (Mantel-Cox) for hMPO-A53T and A53T (***P = 0.0002).

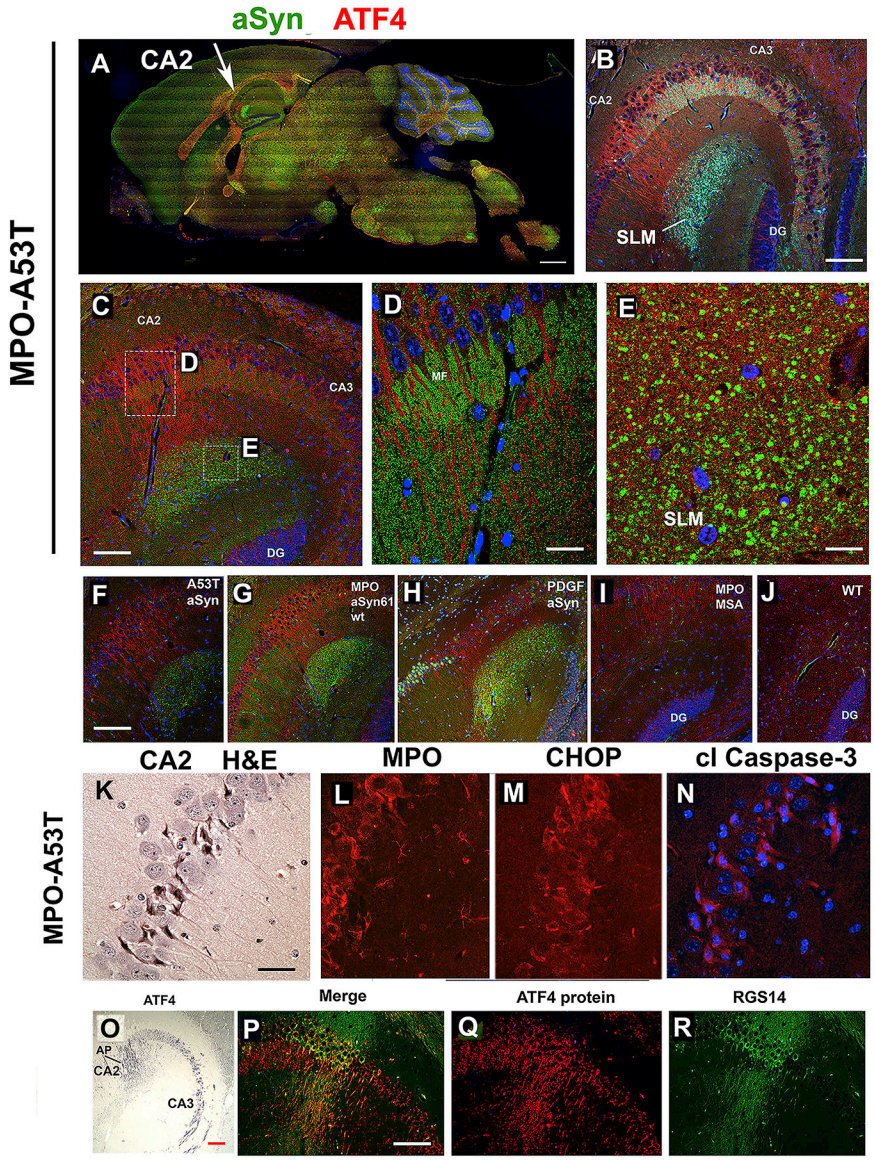

Fig. 10. Accumulation of αSyn aggregates in hippocampal CA2 region associated w ith ATF4 expression in dendrites.

(A) A sagittal section of MPO-A53T brain was immunostained with αSyn505 (green) and ATF4 (red). An arrow points to the hippocampal CA2 region with red and green staining. (B) Higher magnification of the CA2 region shows the dentate gyrus (DG), CA3, and CA2 regions. ATF4 immunostaining (red) is seen in CA2 neurites terminating in a region of αSyn aggregates (green) in the stratum lacunosum moleculare (SLM). (C,D,E) Higher definition confocal image (C) shows two boxed regions in CA2 that are magnified in D and E. (D) ATF4 present in punctate vesicles (red) in CA2 neurites passing through the mossy fiber tract (MF). (E) CA2 neurites with ATF4 (red) passing through larger bead-like aggregates of αSyn (Syn505) (green) in the SLM. (F,G,H) This staining pattern for ATF4 and αSyn aggregates is also seen in A53T brain lacking hMPO, though staining is less intense (F), as well as in the hMPO-Syn61 model (G), and in the PDGF-αSyn model (H). (I) The hMPO-MSA model shows lower level of ATF4 staining in CA2 neurites (red) but lacks the αSyn

aggregates (green). (J) CA2 region from wild-type mice lacks both ATF4 staining and αSyn aggregates. (K) The CA2 region of hMPO-A53T brain is stained with hematoxylin and eosin showing pyknotic neurons. (L,M,N) Immunostaining of MPO-A53T CA2 region for MPO (L), CHOP (M), and cleaved caspase-3 (N). (O) A low magnification image of the hippocampus shows ATF4 immunostaining (black) throughout the CA2 and CA3 soma while only CA2 apical dendrites (AP) express significant ATF4. (P,Q,R) Confocal images show immunostaining of the CA2 region for RGS14 (R), a specific marker for CA2 neurons, ATF4 (Q), and the merged images (P). Scale bars A 1 mm, B 40 μm, C 70 μm, D 15 μm, E 15 μm, F-J 100 μm, K 25 μm, O 30 μm P-R 30 μm. All mice used in these studies were males.

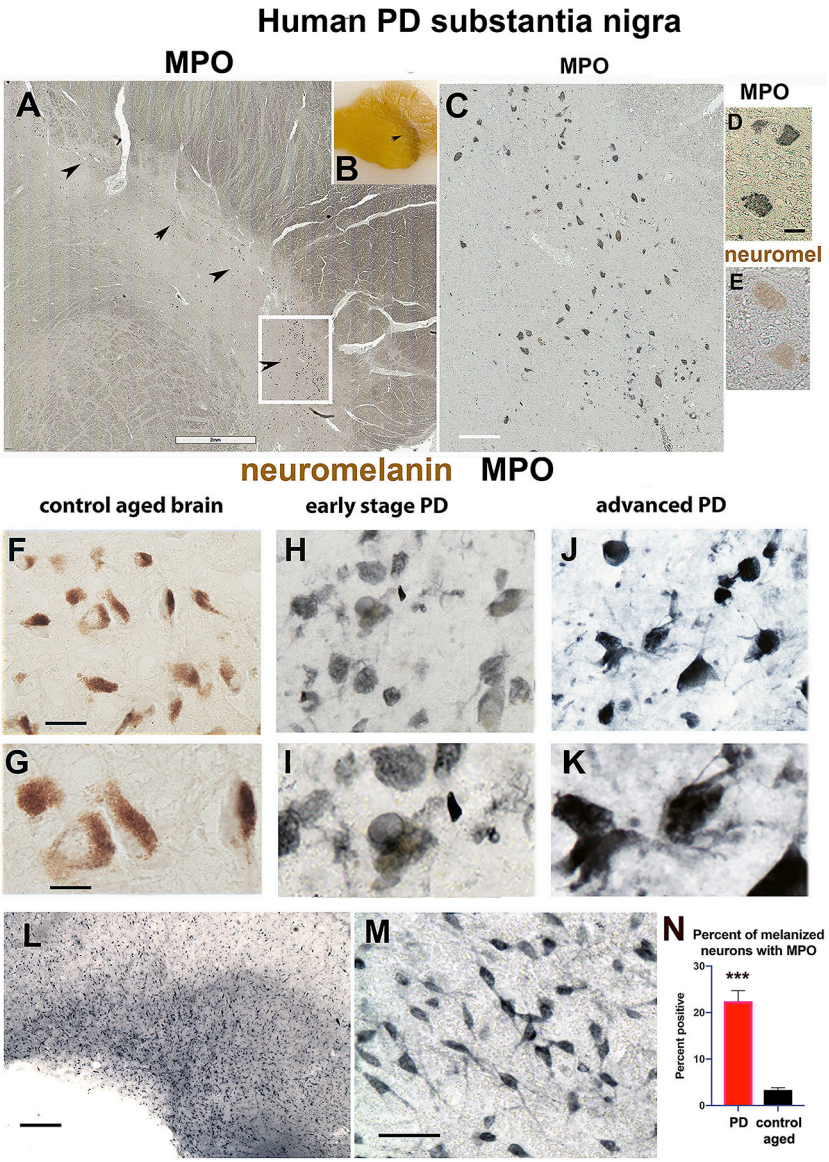

Figure 11. MPO is expressed in neurons in PD substantia nigra.

(A) Sections of PD SNpc were immunostained with anti-MPO antibodies (rabbit polyclonal, Dako) followed by biotinylated secondary antibodies and developed with Vector SG peroxidase substrate (black). Arrowheads denote the tract of melanized neurons. Boxed area is enlarged in panel C. (B) Paraffin block containing control human SNpc with arrow indicating the melanized tract. (C) MPO immunostaining of melanized neurons in PD SNpc at higher magnification. (D) Magnification of MPO immunostained neurons from the melanized tract. (E) Melanized neurons lacking MPO immunostaining showing brown neuromelanin. (F,G) MPO immunostaining (black) of melanized neurons (brown) in control aged brain tissue (F) with higher magnification in G. (H,I) MPO immunostaining (black) in melanized (brown) neurons in the SNpc from early stage PD (H), shown at higher magnification in I. (J,K) MPO immunostaining (black) in dystrophic SNpc neurons exhibiting fibrous dystrophic morphology in advanced stage PD (J), with higher

magnification in K. (L) Low magnification image of an adjacent region showing MPO immunostaining of a different subset of neurons, shown at higher magnification in (M). (N) A minimum of three sections from eight PD and eight normal control SN were analyzed by counting the numbers of melanized neurons with MPO immunostaining, with four areas imaged per section. Representative examples are shown. Scale bar A (2 mm), C (200 μm), D,E (5 μm), F, (20 μm), G (10 μm), L (250 μm), M (50 μm).

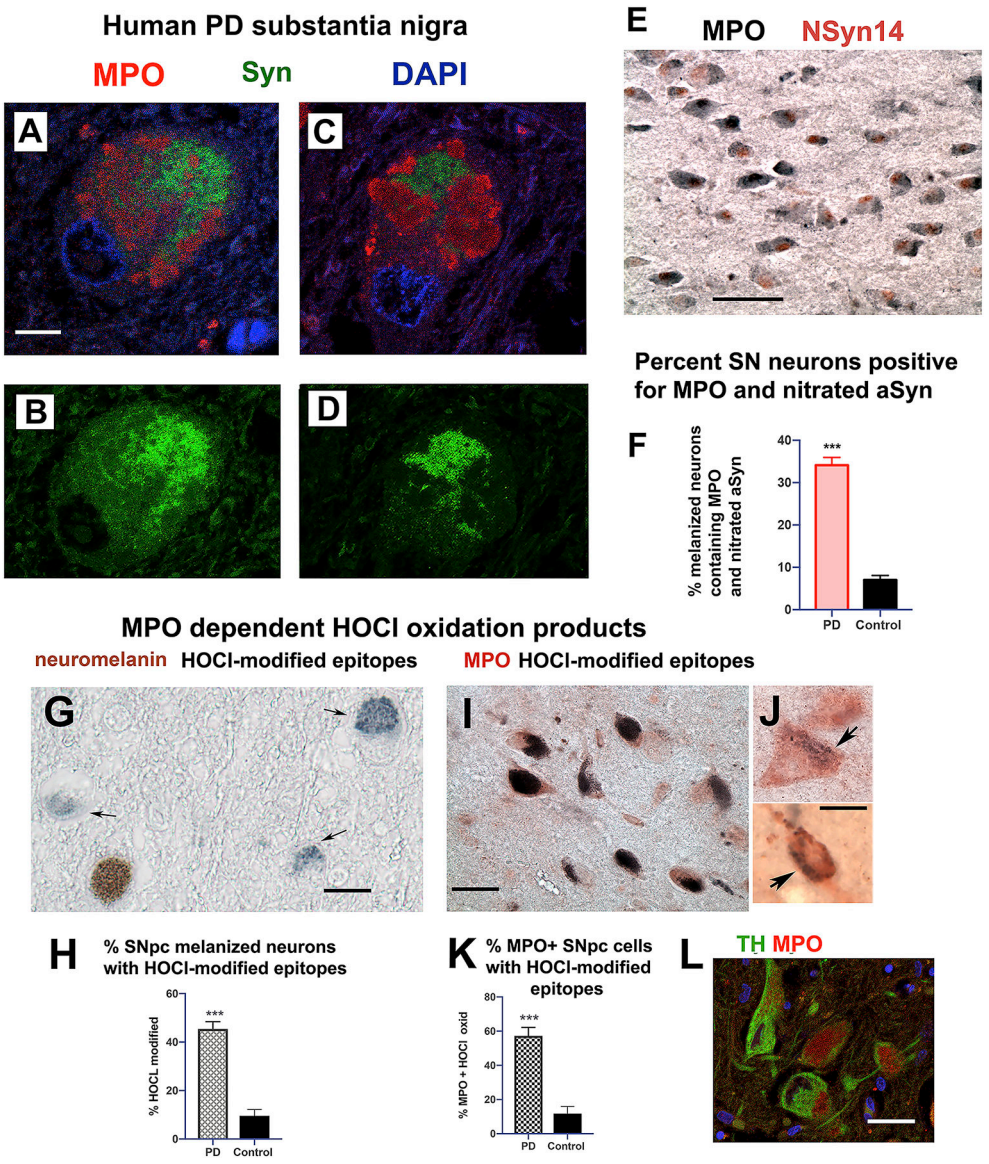

Figure 12. MPO specific HOCl-modification products in melanized neurons in PD SNpc.

(A-D) Two representative examples (A and C) of confocal immunofluorescence staining of neurons from PD SNpc showing MPO (Dako rabbit anti-hMPO, Alexafluor 594, red), αSyn (mouse monoclonal antibody Syn505, Alexafluor 488, green), and DAPI (blue) (63x objective). (B and D) The single green channel immunofluorescence shows αSyn from A and C respectively. (E) Immunoperoxidase staining of MPO (Dako rabbit) and nitrated αSyn (nSyn14)(red) in melanized neurons in human PD SNpc. (F) Quantitation of percent of melanized neurons in human PD SNpc and aged control SN that costain for both MPO and nitrated αSyn. (G, I, J) Monoclonal antibody 2D10G9 detects HOCl-modified epitopes (black, arrows) in melanized neurons (G). (H) Quantitation of neuromelanin containing neurons positive for HOCl-modified epitopes in PD SNpc versus control SNpc. (I,J) Immunostaining for MPO (red) in melanized neurons that also show positive staining for HOCl-modified epitopes using 2D10G9 (black) (arrows denote small vesicles positive for

HOCl epitopes). (K) Quantitation of MPO positive neurons with HOCl epitopes in PD SNpc versus control aged SNpc. (L) Confocal image of MPO immunostaining (red, AlexaFluor 594) in neurons with tyrosine hydroxylase (green, AlexaFluor 488), a marker for dopaminergic neurons. These immunohistological studies assayed eight PD SN and eight normal control SN. In E and F, percent of immunopositive cells was determined from a minimum of three sections from each donor, spaced by five sections, with four digital images analyzed from each section. Counting of immunopositive neurons was performed by investigators blinded to PD or control status. Statistical significance in F, H, and K was determined by Student's t test. Scale bars A (5 μm), C (10 μm), E (40 μm), G (5 μm), I (15 μm), J (10 μm), L (15 μm).